Effect of slope aspect on transformation of clay minerals in Alpine soils

Egli, Markus ; Mirabella, A ; Sartori, G ; Giaccai, D ; Zanelli, R ; Plötze, M

Abstract: Two soil profile sequences on paragneiss debris in the Val di Rabbi (Northern Italy) along an altitude gradient ranging from 1200 to 2400 m a.s.l. were studied to evaluate the effect of aspect on the weathering of clay minerals. All the soils had a coarse structure, a sandy texture and a low pH. Greater weathering intensities of clay-sized phyllosilicates (greater content of smectites) were observed in soils on the north-facing slope. On the south-facing slope, smectite was found only in the surface horizon of the soil profile at the highest altitude. Hot citrate treatment of north-facing soils revealed the presence of low-charged 2:1 clay minerals, the expansion of which was hindered in the untreated state by interlayered polymers. However, the hot citrate treatment encountered some problems with the samples of the south-facing soils: as confirmed by Fourier transform infrared spectroscopy, the hot citrate treatment was unable to remove all interlayer Al polymers. The 2:1 phyllosilicates were not expanded by ethylene glycol solvation in several samples, although thermogravimetric analyses indicated the presence of clay minerals with interlayer H O. At the same time, the collapse of clay minerals to 1.0 nm following K-saturation was evident. Theoretically, this should indicate that 2:1 phyllosilicates had no evident substitution of trioctahedral cations (Mg^{2} , Fe^{2}) by dioctahedral cations (Al^{3} and Fe^{3}). X-ray diffraction analysis of the d060 region and determination of the layer charge of clay minerals by the long-chain (C) alkylammonium ion, however, did not confirm this. A transformation from trioctahedral to dioctahedral species was observed and low-charge clay minerals (0.30) were identified in the surface horizons of the south-facing sites. In the south-facing soils, the podzolization process was less pronounced because of a lower water flux through the soil and probably less complexing organic molecules that would remove the interlayer polymers. Besides the eluviation process, clay minerals underwent a process of ionic substitutions in the octahedral sheet that led to the reduction of the layer charge. This process was more obvious in the north-facing sites.

DOI: https://doi.org/10.1180/claymin.2007.042.3.09

Clay Minerals, (2007) **42**, 373–398

Effect of slope aspect on transformation of clay minerals in Alpine soils

M. EGLI[1,*], A. MIRABELLA[2], G. SARTORI[3], D. GIACCAI[2], R. ZANELLI[1] AND M. PLÖTZE[4]

[1] *Department of Geography, University of Zurich, Winterthurerstrasse 190, 8057 Zurich, Switzerland,* [2] *Istituto Sperimentale per lo Studio e la Difesa del Suolo, Piazza D'Azeglio 30, 50121 Firenze, Italy,* [3] *Museo Tridentino di Scienze Naturali, Via Calepina 14, 38100 Trento, Italy, and* [4] *ETH Zurich, Institute for Geotechnical Engineering, 8093 Zurich, Switzerland*

(*Received 2 January 2007; revised 21 June 2007*)

ABSTRACT: Two soil profile sequences on paragneiss debris in the Val di Rabbi (Northern Italy) along an altitude gradient ranging from 1200 to 2400 m a.s.l. were studied to evaluate the effect of aspect on the weathering of clay minerals. All the soils had a coarse structure, a sandy texture and a low pH. Greater weathering intensities of clay-sized phyllosilicates (greater content of smectites) were observed in soils on the north-facing slope. On the south-facing slope, smectite was found only in the surface horizon of the soil profile at the highest altitude. Hot citrate treatment of north-facing soils revealed the presence of low-charged 2:1 clay minerals, the expansion of which was hindered in the untreated state by interlayered polymers. However, the hot citrate treatment encountered some problems with the samples of the south-facing soils: as confirmed by Fourier transform infrared spectroscopy, the hot citrate treatment was unable to remove all interlayer Al polymers. The 2:1 phyllosilicates were not expanded by ethylene glycol solvation in several samples, although thermogravimetric analyses indicated the presence of clay minerals with interlayer H_2O. At the same time, the collapse of clay minerals to 1.0 nm following K-saturation was evident. Theoretically, this should indicate that 2:1 phyllosilicates had no evident substitution of trioctahedral cations (Mg^{2+}, Fe^{2+}) by dioctahedral cations (Al^{3+} and Fe^{3+}). X-ray diffraction analysis of the d_{060} region and determination of the layer charge of clay minerals by the long-chain (C_{18}) alkylammonium ion, however, did not confirm this. A transformation from trioctahedral to dioctahedral species was observed and low-charge clay minerals (ξ ~0.30) were identified in the surface horizons of the south-facing sites. In the south-facing soils, the podzolization process was less pronounced because of a lower water flux through the soil and probably less complexing organic molecules that would remove the interlayer polymers. Besides the eluviation process, clay minerals underwent a process of ionic substitutions in the octahedral sheet that led to the reduction of the layer charge. This process was more obvious in the north-facing sites.

KEYWORDS: smectite, Na-citrate treatment, weathering, soils, microclimate, aspect.

Various environmental conditions determine differing soil formations, with several factors influencing the weathering rates of soils. These are in particular the parent material, climate, topography, time and organisms (Jenny, 1980).

* E-mail: megli@geo.unizh.ch
DOI: 10.1180/claymin.2007.042.3.09

In recent years, several studies have been carried out on soils developing in Alpine environments in order to investigate the role of individual factors. The various (silicate) lithologies of the parent material led to differences in the clay mineral assemblages in weathered soils, with smectite developing on granites, granodiorite and tonalite, whereas interstratified mica-vermiculite formed from slate glacial till (Mirabella *et al*., 2002). The

main clay mineral transformations usually occurred within the first 3000 y of soil development (Righi *et al*., 1999; Egli *et al*., 2001a,b, 2003a). Climate, a factor of growing interest because of its currently-occurring worldwide change, affected clay mineral transformations with smectite being detected in the upper mountain belt and in the subalpine belt up to the timberline (1400–1900 m a.s.l.). Most of the soils studied were located on north-facing slopes (Mirabella & Sartori, 1998; Mirabella & Egli, 2003; Egli *et al*. 2003b, 2004).

In Alpine areas, the most weathered and typical soils are podzols that show characteristic eluviation and illuviation features of Fe, Al and organic carbon (De Coninck, 1980; Anderson *et al*., 1982; Farmer, 1982). They usually develop in cool and moist climates in the northern or southern hemisphere (Dahlgren & Ugolini, 1991; Gustafsson *et al*., 1995), but examples of their presence in the cool humid environments of the tropics have also been cited (Van Ranst *et al*., 1997). In particular, precipitation and temperature may influence the type and rate of soil chemical, biological and physical processes, and have a significant impact on the global geochemical cycle (Bain *et al*., 1994; Dahlgren *et al*., 1997).

Greater precipitation rates and the production of chelating compounds in the soil are believed to promote the development of smectites, which seem to be the weathering end-products of the phyllosilicates mica or chlorite through the intermediate stage of hydroxy-interlayered minerals and the subsequent removal of the hydroxide polymers (Malcolm *et al*., 1969; Senkayi *et al*., 1981; Carnicelli *et al*., 1997; Righi *et al*., 1999; Egli *et al*., 2003b). As early as 1967 and 1970, Gjems deduced from X-ray diffraction (XRD) analysis of clay minerals of podzols that smectites (then designated montmorillonite) form in the E horizon at the expense of chlorite, illite or vermiculite, and that mixed-layer minerals become less chloritic upwards within the profile. Additionally, it was shown that the smectite content increased upwards within the soil profile inversely with trioctahedral mica, chlorite, mica-chlorite and mica-vermiculite interstratified minerals.

Earlier studies documented the effect of differences in climate along an elevational gradient (leading to an upward decrease in temperature and generally an increase in precipitation) on plant communities and soils. Common trends reported in these studies included changes in soil types, soil organic matter, clay content, soil acidity and exchangeable ions (e.g. Whittaker *et al*., 1968; Mahaney, 1978; Laffan *et al*., 1989; Bäumler & Zech, 1994; Bockheim *et al*., 2000; Sartori *et al*., 2005). The influence of slope aspect and the resulting microclimate has been the subject of several investigations (Cooper, 1960; Klemmedson, 1964; Macyk *et al*., 1978; Hunckler & Schaetzl, 1997; Rech *et al*., 2001). The results obtained by these authors were not unequivocal. Some measured greater chemical weathering on south-facing soils and some on north-facing soils. Furthermore, none of these studies documented the effect of the slope on the structural transformations of clay minerals.

We therefore carried out the present study to shed light on the mechanisms involved in the

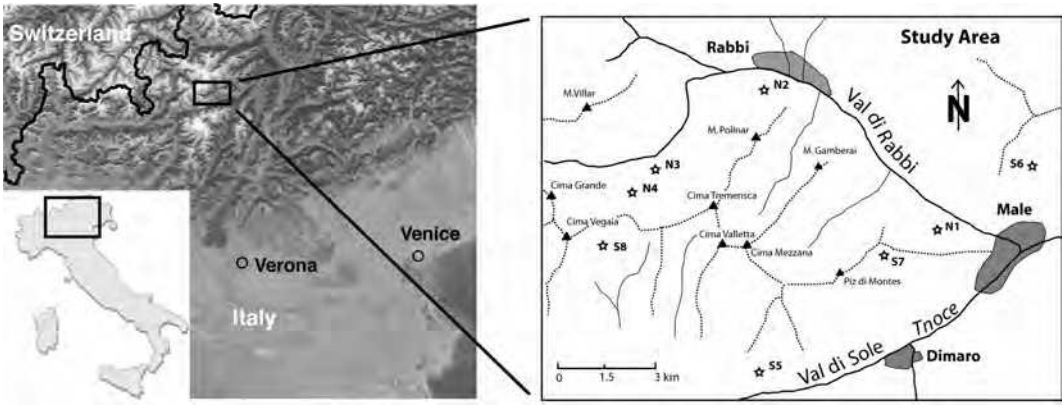

FIG. 1. Location of Val di Rabbi and of the investigation sites N1–4 (N for north-facing) and S5–8 (S for south-facing).

transformation and weathering of clay minerals as influenced by the different facing of soils developing on paragneiss in an Alpine area of Northern Italy.

INVESTIGATION AREA

Two soil sequences in the Val di Rabbi (Northern Italy; Fig. 1), along an altitude gradient ranging from 1200 to 2400 m a.s.l., were investigated (Table 1). The two sequences exhibit different exposition: one was north-facing and the other south-facing. The soil profiles are assumed to be representative of the elevational zones and were selected during an ongoing detailed soil survey. Care was taken to select natural and undisturbed sites. The soil profiles exhibited no signs of erosion or accumulation. Because the selection of undisturbed soils was the main prerequisite, not all sites had an identical slope angle. Climate (temperature and precipitation) varied along the toposequence and consequently so did vegetation. Coniferous forest was found up to an altitude of 2000 m a.s.l. and alpine meadow at higher altitudes. The sites showed the typical vegetation types for the corresponding altitude and exposure (Pedrotti *et al*., 1974). At lower altitudes, north-facing sites had coniferous forests with predominantly white fir while at south-facing sites mixed forests (deciduous and coniferous trees) were encountered. At higher altitudes, coniferous forests with larch and spruce fir dominated at both north- and south-facing sites. Above the timberline, alpine meadow was the typical vegetation type.

The soils varied, according to the World Reference Base for Soil Resources (FAO, 1998), from Dystric Cambisols to Episkeleti-Endoleptic or Endoskeletic Podzols (Table 1). They had developed on paragneiss debris or morainic material consisting of paragneiss (migmatitic paragneiss of

TABLE 1. Characteristics of the two study sequences in Val di Rabbi, Southern Alps.

Profile	Elevation (m a.s.l.)	Aspect (ºN)	Slope (º)	Parent material	Vegetation	Land use	WRB (FAO, 1998)
North-facing sites							
N1	1180	340	31	Paragneiss-debris	*Abietetum albae*	Natural, coniferous (white fir) forest (ecological forestry)	Chromi-Episkeletic Cambisol (Dystric)
N2	1620	0	29	Paragneiss-debris	*Piceetum montanum*	Natural, coniferous forest (ecological forestry)	Chromi-Endoskeletic Cambisol (Dystric)
N3	1910	20	12	Paragneiss-glacial deposits	*Nardetum alpigenum*	Occasionally used as pasture; natural, coniferous forest	Episkeletic Podzol
N4	2390	30	25	Paragneiss-debris	*Rhodoro - vaccinietum extrasilvaticum*	Natural grassland and shrubs	Enti-Umbric Podzol (Episkeletic)
South-facing sites							
S5	1185	160	31	Paragneiss-debris	*Orno-ostryon*	Ex-coppice; natural, mixed forest (ecological forestry)	Episkeleti-Endoleptic Cambisol (Chromi-Dystric)
S6	1660	210	33	Paragneiss-debris	*Larix decidua*	Natural, coniferous forest (ecological forestry)	Skeletic Umbrisol
S7	1995	160	25	Paragneiss-rock outcrop/debris	*Larix decidua/Picea abies*	Ex-pasture, natural, coniferous forest	Skeletic Umbrisol
S8	2420	190	28	Paragneiss- rock outcrop/debris	*Festucetum*	Natural grassland	Dystri-Epileptic Cambisol

the Ulten-Tonale zone; Bosselini *et al*., 2002). The primary mineralogical composition was similar at all sites. Primary minerals were quartz (high abundance), plagioclase (medium to high abundance), biotite (medium to high abundance), muscovite (medium abundance), chlorite and HIV (low to medium abundance) and K-feldspar (low abundance). At site S7, there were also measurable traces of talc. At sites S7 and S8, both rock outcrops and rock debris occurred in the surrounding area, and soils that had developed on rock debris were sampled. The climate ranged from temperate to alpine. According to Soil Taxonomy (USDA and NRCS, 2006), the soil moisture regime was udic (humid conditions, <90 days/y with a dry soil) at all sites and the soil temperature regime varied between frigid (mean annual temperature <8ºC) and cryic (mean annual temperature <8ºC, no permafrost). Maximum precipitation occurs during the summer months. The mean annual temperature and precipitation in nearby Peio (1580 m a.s.l.) are 6.8ºC and 861 mm/y, respectively. In Val di Rabbi, the mean annual temperature ranges from 8.2 (valley floor) to around 0ºC (at 2400 m a.s.l.), and mean annual precipitation is ~800–1300 mm/y (Servizio Idrografico, 1959; Sboarina & Cescatti, 2004).

According to the geomorphological study of Baroni & Carton (1990), local soil ages range from 12,000 to 16,000 y.

Vegetation is not a fully-independent soil-forming factor. In this case the distribution of the vegetation along the toposequence (investigated sites) is driven ultimately by the (micro)climate. As the north sequence was directly compared to the south sequence, a pair-wise comparison was performed (with similar vegetation types). Due to the limited differences in the soil age, the similarity of the parent materials and the relatively stable climatic conditions during soil formation, the changes in the weathering processes in the soils can be attributed primarily to the factor climate, influenced both by the altitude and the differing slope facing.

MATERIALS AND METHODS

Soil material was collected from excavated profile pits, air-dried and sieved to <2 mm. The particle-size distribution was determined by sieving the coarser particles (2000–32 μm) and measuring the finer fraction with the pipette method, after pre-treatment of the samples with unbuffered H_2O_2 (3%) and heating, dispersion with Calgon and sedimentation in deionized water. Soil pH was determined by potentiometry in water and a 0.01 M $CaCl_2$ solution, using a soil:solution ratio of 1:2.5. Total C and N contents of the soil were measured with a C/H/N analyser (Elementar Vario EL). Oxalate-soluble Al, Fe and Si were extracted by NH_4-oxalate at pH 3 (Al_o, Fe_o, Si_o) (Schwertmann, 1964). Additionally, the pyrophosphate-extractable fraction was measured (McKeague *et al*., 1971), which is often used to characterize the organically-bound Al fraction. 'Imogolite-type material' (ITM), which henceforth refers to the sum of imogolite and proto-imogolite allophane, was estimated (assuming that the Al/Si molar ratio to be close to 2.0) according to Parfitt & Henmi (1982), i.e. as allophane + imogolite% = Si(oxalate)% × 7.1. Its presence was furthermore checked with Fourier transform infrared spectroscopy (FTIR) (see below). The molar ratio $(Al_o - Al_p)/Si_o$ with Al_o as the oxalate-extractable Al, Al_p as the pyrophosphate-extractable Al, and Si_o as the oxalate-extractable Si_o gave further indications of the presence of ITM. Element pools in the soil (Ca, Mg, K, Na, Fe, Al, Mn, Si and Ti) were determined by a method of total digestion. Oven-dried (70ºC) samples were dissolved using a mixture of HF, HCl, HNO_3 and H_3BO_3 in a closed system (microwave-oven and under high pressure, 25 bar). Concentrations of Ca, Mg, K, Na, Fe, Mn, Al, Si and Ti were determined by atomic-absorption spectroscopy, in part using a graphite furnace.

To separate the clay fraction (2 μm), the fine earth samples (<2 mm) were pre-treated at room temperature with diluted and Na-acetate buffered (pH 5) H_2O_2. At the end of the reaction, H_2O_2 was decomposed by heating the sample at 50ºC. The clay fraction was obtained by dispersion with Calgon and sedimentation in water. Specimens were then saturated with Mg, washed free of chloride and freeze-dried. Clay-aggregate samples, oriented on glass slides from a water suspension, were analysed using a 3 kW Rigaku D/MAX III C diffractometer, equipped with a horizontal goniometer and a graphite monochromator, using Cu-*K*α radiation. Slides were step-scanned from 2 to 15º2θ with steps of 0.02º2θ at 2 s intervals. The following treatments were performed: Mg-saturation, ethylene glycol-solvation and K-saturation, followed by heating for 2 h at 335ºC and 550ºC. The whole mineralogical composition of the clay fraction was

checked with randomly-oriented specimens (PHILIPS PW1820; Cu-$K\alpha$, 40 kV, 30 mA, 4–70º2θ, 0.02º2θ steps, 3 s per step, automatic slits). When chlorite was present, the presence of kaolinite was checked with FT-IR (Brooker Optics, Tensor 27) analysis (OH-stretching region near 3690 cm^{-1}) on pellets made with 1 mg of sample and 150 mg of KBr heated at 150ºC. Digitized X-ray data were routinely smoothed and corrected for Lorentz and polarization factors (Moore & Reynolds, 1997). Diffraction patterns were smoothed by a Fourier transform function and fitted by the Origin™ PFM program using the Pearson VII algorithm. Background values were calculated by means of a non-linear function (polynomial 2nd order function; Lanson, 1997).

The d_{060} region was studied on random mounts prepared by back-filling Al holders and gently pressing over filter paper and then step-scanned from 58 to 64º2θ with steps of 0.02º2θ at 10 s intervals. Layer-charge estimation of smectites was performed using the long-chain (C_{18} and C_{12}) alkylammonium ions according to the method proposed by Olis *et al*. (1990).

For the monolayer to bilayer transition, the following equation was used:

$$C_{18}: d_{001} = 8.21 + 34.22\xi$$
$$C_{12}: d_{001} = 5.52 + 32.98\xi$$

with ξ = mean layer charge and d values given in Å.

For the bilayer to pseudotrimolecular layer transition, the equation is:

$$C_{18}: d_{001} = 8.71 + 29.65\xi$$
$$C_{12}: d_{001} = 8.71 + 20.25\xi$$

Na-citrate treatment was performed to extract hydroxy-Al (or Fe) from the interlayers of 2:1 clay minerals. The procedure according to Tamura (1958) was applied in a modified form, in which a contact time of 24 h without extractant removal was obtained by heating the samples in an autoclave at 135ºC. After the Na-citrate procedure, the following treatments were performed: Mg-saturation, ethylene glycol solvation and K-saturation, followed by heating for 2 h at 335ºC and 550ºC. The XRD patterns of the treated samples were then compared with those of the corresponding untreated samples. To check the influence of the Na-citrate treatment on the phyllosilicate structures, the FTIR spectra of soil clays (before and after the treatment) in the OH-bending region were first normalized (min-max method) in the M–O region (900–400 cm^{-1}) and then compared to each other.

Thermogravimetric analyses were carried out with a Mettler-Toledo TGA/SDTA 851[e] instrument by dynamic heating to 1000 C (rate 10 K/min) using ~40 mg of sample in a 150 µl Pt pan with 50 cm^3/min dry and decarbonated air as purging gas. Linking the instrument with a quadrupole mass spectrometer (Balzers Thermostar) allowed the determination of the gases released at defined temperatures. For clays, reactions at lower temperatures (<250ºC) involve, for example, desorption of surface water and dehydration of phyllosilicate interlayers, whereas at elevated temperatures (450–900ºC) dehydroxylation (release of the octahedral OH and destruction of the clay mineral structure) occurs. Gases evolved from soil material, other than the H_2O from these reactions, are commonly H_2O and CO_2 from organic matter (e.g. Karathanasis & Harris, 1994).

RESULTS

Physical and chemical analyses

The thickest soil columns at the north-facing sites were found at 1200–1620 m a.s.l. and at the south-facing sites at 1400–1995 m a.s.l. At the lower south-facing sites up to ~1400 m a.s.l. and at the highest site the soils are Cambisols (Skeletic to Leptic), and at the other sites they are Umbrisols (Table 1). Most of the soils at the north-facing sites and at the south-facing sites at higher elevations showed typical podzolic characteristics but cannot be classified as Podzols because the B horizon does not fully meet the prerequisites of a spodic horizon. The investigated soils have a comparatively high proportion of soil skeleton that varies from 30% to 80% of the mass (Table 2). These are typical values for Alpine soils on debris or morainic substratum (Egli *et al*., 2001b).

The soils exhibited a sandy loam to loamy texture; the proportion of sand decreased towards the soil surface, and correspondingly silt and clay increased (Table 2). The upward decrease of the grain sizes is a concomitant effect of weathering, although an aeolian addition after the retreat of the glaciers (~15,000–17,000 years BP) in the last glaciation phase (cf. Bäumler & Zech, 1994) or by southerly winds carrying Sahara dust cannot be fully excluded. The errors introduced by any inhomogeneities seem, however, to be of minor

TABLE 2. Some physical properties of the investigated soils.

Site and soil horizons	Coarse sand (wt.%)	Fine sand (wt.%)	Coarse silt (wt.%)	Fine silt (wt.%)	Sand (wt.%)	Silt (wt.%)	Clay (wt.%)	Skeleton (wt.%)	Density (g cm^{-3})
North-facing sites									
Profile N1 1180 m a.s.l.									
AE	26	1.3	32.8	21.2	27.3	54	18.7	50	1.13
EB	30.2	19.4	14.9	20.9	49.6	35.8	14.6	n.d.	n.d.
Bs1	30.5	12.3	26.0	19.8	42.8	45.8	11.4	56	1.26
Bs2	63	9.2	12.0	10.4	72.2	22.4	5.4	74	1.39
BC	57.5	22.2	4.1	9.4	79.7	13.5	6.8	76	1.67
Profile N2 1620 m a.s.l.									
E	28	8.0	23.0	25.0	36.0	48.0	16.0	35	0.96
Bs1	30.5	9.5	34.0	18.5	40.0	52.5	7.5	67	1.21
Bs2	50	12.5	16.0	16.5	62.5	32.5	5.0	80	1.46
BC	60.5	14.6	12.0	10.0	75.1	22.0	2.9	n.d.	n.d.
C		n.d.	n.d.	n.d.	n.d.	n.d.	n.d.	60	1.71
Profile N3 1910 m a.s.l.									
EA	29	9.0	28.0	16.0	38.0	44.0	18.0	0	0.63
E	32.8	19.0	16.7	16.9	51.8	33.6	14.6	0	0.63
Bhs	41	9.9	24.0	12.6	50.9	36.6	12.5	29	1.13
Bs	49	12.9	23.5	8.7	61.9	32.2	5.9	43	1.13
BC	53.3	21.3	10.7	11.2	74.6	21.9	3.5	n.d.	n.d.
C	57.2	18.4	7.4	13.6	75.6	21.0	3.4	63	1.77
Profile N4 2390 m a.s.l.									
OE	24.8	4.3	29.6	17.0	29.1	46.6	24.3	9	0.57
BE	40.3	18.2	17.0	12.0	58.5	29.0	12.5	59	1.1
Bhs	58	18.0	11.0	8.4	76.0	19.4	4.6	70	0.98
BC	62	17.0	9.0	8.0	79.0	17.0	4.0	79	1.8
South-facing sites									
Profile S5 1185 m a.s.l.									
A	44	5.4	8.2	30.6	49.4	38.8	11.8	21	n.d.
Bw1	41	16.5	13.0	18.0	57.5	31.0	11.5	32	1.14
Bw2	59	6.6	15.0	13.0	65.6	28.0	6.4	49	1.4
C	64	12.5	10.5	10.0	76.5	20.5	3.0	74	1.9
Profile S6 1660 m a.s.l.									
AE	32	17.0	19.5	17.5	49.0	37.0	14.0	16	0.82
Bs1	32	17.5	19.0	21.0	49.5	40.0	10.5	24	1.13
Bs2	53	6.5	26.0	11.5	59.5	37.5	3.0	50	1.24
BC	57	22.7	8.5	9.0	79.7	17.5	2.8	69	1.35
Profile S7 1995 m a.s.l.									
AE	26	15.5	3.5	33.5	41.5	37.0	21.5	1	0.7
BA	25	12.5	40.0	12.0	37.5	52.0	10.5	42	1.42
Bs1	55	9.2	21.6	9.8	64.2	31.4	4.4	42	1.42
Bs2	68	13.0	9.6	8.0	81.0	17.6	1.4	33	1.61
BC	55	14.0	17.0	12.5	69.0	29.5	1.5	n.d.	n.d.
C	40	10.0	27.0	20.5	50.0	47.5	2.5	42	1.8
Profile S8 2420 m a.s.l.									
OE	35.5	13.0	18.0	16.0	48.5	34.0	17.5	1	0.48
Bs	56	11.0	13.0	12.5	67.0	25.5	7.5	39	1.15
BC	66	5.0	21.0	6.0	71.0	27.0	2.0	24	1.4

Coarse sand: 2000−200 μm; fine sand: 200−50 μm; coarse silt: 50−20 μm, fine silt: 20−2 μm, clay <2 μm
n.d. = not determined; skeleton fraction >2 mm

importance. The possible aeolian contribution was not particularly high, as the fine sand fraction in the parent material was higher in the C horizons of most soils than in the topsoils (Table 2). Also, investigations of the mineralogy, particle-size fraction and major element chemistry in a neighbouring area (Egli *et al*., unpublished data) showed that aeolian additions are difficult to detect.

The pH was low, the most acidic conditions being found in the surface horizon. The characteristic eluviation of Al and Fe (oxalate- as well as dithionite-extractable fraction, see Table 3) was encountered in the north-facing N2, N3 and N4 soil profiles and, less evidently, in the south-facing S6, S7 and S8 soil profiles. The amount of imogolite-type material was furthermore quite low in all soil profiles (Table 3). Small amounts of imogolite-type materials (ITM) were observed in the lower horizons of the profile at 1620 m a.s.l. on the north-facing sequence and in the whole B horizon of the two soils at 1660 and 1996 m a.s.l. on the south-facing sequence (Table 3).

The total element contents of the investigated soils showed a paragneiss-like composition (Table 4). The chemical compositions of the C horizons between the sites were quite homogeneous, with Al_2O_3 in the parent material slightly higher at the south-facing sites, while no difference could be measured for all other components between the north- and south-facing sites. The main mineralogical compositions (except for the different clay minerals) in the clay fraction were almost identical between the sites (data not shown). The clay fractions were characterized by phyllosilicates, K-feldspar, plagioclase and quartz. These results show that the variation of the state-factor parent material (Jenny, 1980) is small.

Clay mineral analyses

North sequence. An overview of the detected clay minerals is given in Table 5. An XRD pattern of the EG-solvated clay sample from the AE horizon of soil profile N1 at 1200 m a.s.l. showed three fundamental reflections at 1.41, 1.01 and 0.71 nm (Fig. 2). The decomposition procedure allowed separation of the wide peak at 1.41 nm into three components: a small peak at 1.71 nm, representing smectite, a large peak at 1.41 and another one at 1.20 nm. A further minor peak was located at 2.54 nm (Fig. 2). Mg- and K-saturation and the subsequent heating treatments allowed the identification of vermiculite (1.41 nm, Mg-saturation), hydroxy-interlayered vermiculite (HIV; 1.41 nm, Mg-saturation), regularly-interstratified mica-HIV (with d_{001}* and d_{002}* at 2.54 and 1.20 nm, respectively, Mg-saturation) and traces of chlorite. Due to the reflection at a low angle we must assume that mica-HIV is mostly regularly-interstratified (R1). The other phyllosilicates present in this sample were mica and kaolinite. No smectite was detected in the lower EB horizon (data not shown). A small amount of vermiculite, hydroxy-interlayered vermiculite and irregularly-interstratified chlorite-HIV were present, together with mica, kaolinite and a small amount of chlorite. The mineralogical composition of the Bs1 horizon was very similar to that of the EB horizon, with the exception of the absence of vermiculite. An XRD pattern of the EG-solvated clay sample from the Bs2 horizon showed an increase of the mica peak at 1.01 nm and a corresponding decrease of the peak at 1.41 nm (Fig. 2) and the kaolinite 001 peak at 0.71 nm, when compared with the previously described samples. The other minerals present were hydroxy-interlayered vermiculite and irregularly-interstratified mica-HIV. Chlorite was present in traces. The clay sample from the BC horizon was similar to the Bs2 horizon.

The Mg-saturated clay sample from the E horizon of soil profile N2 exhibited five peaks at 2.55, 1.47, 1.27, 1.02 and 0.72 nm (Fig. 2); furthermore, two other small peaks were evident at 0.85 and 0.92 nm. Following EG-solvation, peaks at 2.55, 1.47 and 1.27 nm were shifted towards lower angles at 2.74, 1.71 and 1.46 nm (Fig. 2). Potassium-saturation caused the peaks at 1.47 and 1.27 nm in the Mg-saturated sample to contract to 1.27 and 1.12 nm, respectively. All these peaks collapsed to 1.02 nm after heating at 335ºC. In this sample, two low-charge expandable minerals could be identified. The first is a smectite represented by the d_{001}* and d_{002}* basal reflections at 1.71 and 0.85 nm. The second is a regularly-interstratified mica-smectite with d_{001}*, d_{002}* and d_{003}* basal reflections at 2.74, 1.46 and 0.92 nm. Mica was present in small amounts and was noticeably weathered (Fig. 2). Mg-saturated and EG-solvated clay samples from the Bs1 horizon exhibited XRD patterns characterized by the peaks centred at 2.43, 1.46, 1.27, 1.02 and 0.72 nm (Fig. 2). The mica peak was quite broad and weak. A portion of the peak at 1.46 nm shifted towards 1.02 nm with the heating treatment at 335ºC. Only a fraction of this peak collapsed to

TABLE 3. Main chemical characteristics of the investigated soils.

Site and soil horizons	pH ($CaCl_2$)	pH (H_2O)	Organic C (g/kg)	Al_d[1] (g/kg)	Fe_d (g/kg)	Al_o[1] (g/kg)	Fe_o (g/kg)	Si_o (g/kg)	Al_p[1] (g/kg)	ITM (g/kg)	Molar ratio $(Al_o-Al_p)/Si_o$
North-facing sites											
Profile N1 1180 m a.s.l.											
AE	3.5	4.5	25.5	2.65	19.58	3.45	9.11	0.96	1.97	6.8	1.61
EB	n.d.	4.9	19.6	n.d.	n.d.	n.d.	n.d.	n.d.	n.d.	n.d.	
Bs1	4	5.1	14.9	3.34	18.45	3.40	6.97	0.84	2.82	6.0	0.72
Bs2	4.3	5.2	6.9	2.83	23.74	2.70	6.07	0.52	1.97	3.7	1.46
BC	4.1	5.6	3.7	1.26	27.57	1.01	3.75	0.22	n.d.	1.6	
Profile N2 1620 m a.s.l.											
E	3	3.5	56.5	2.75	23.72	3.12	6.56	0.24	2.32	1.7	3.47
Bs1	4.2	5.1	23.1	6.79	38.43	5.78	9.53	1.00	6.41	7.1	–0.66
Bs2	4.6	5.6	16.0	8.89	40.81	11.14	13.16	3.33	4.44	23.6	2.09
BC	n.d.	5.7	4.4	n.d.	n.d.	n.d.	n.d.	n.d.	n.d.	n.d.	
C	4.7	5.9	2.7	1.73	13.55	2.12	2.53	0.51	n.d.	3.6	
Profile N3 1910 m a.s.l.											
EA	3.9	4.6	194.2	8.68	15.14	9.70	11.56	0.11	9.19	0.8	4.83
E	n.d.	4.3	82.0	n.d.	n.d.	n.d.	n.d.	n.d.	n.d.	n.d.	
Bhs	4	4.5	66.4	14.59	31.58	13.50	20.16	0.37	14.48	2.6	–2.76
Bs	4.3	4.6	28.0	15.29	23.71	14.46	12.45	1.33	13.50	9.4	0.75
BC	n.d.	4.7	10.1	n.d.	n.d.	n.d.	n.d.	n.d.	n.d.	n.d.	
C	4.5	5.0	7.2	3.73	15.46	3.38	3.86	0.98	n.d.	7.0	
Profile N4 2390 m a.s.l.											
OE	3.5	4.1	151.4	2.66	15.61	2.80	5.39	<0.02	2.88	n.d.	
BE	4.1	4.6	69.3	8.01	33.20	9.00	17.45	0.12	6.80	0.9	19.09
Bhs	4.3	5.2	38.8	9.97	33.25	10.12	16.03	0.60	9.49	4.3	1.09
BC	4.6	5.3	18.4	6.60	27.22	7.22	5.05	1.49	n.d.	10.6	
South-facing sites											
Profile S5 1185 m a.s.l.											
A	4.4	5.3	28.4	1.95	17.29	1.17	3.23	0.28	1.33	2.0	–0.59
Bw1	4	5.0	13.2	2.33	20.22	1.32	3.68	0.17	1.10	1.2	1.35
Bw2	3.9	5.2	9.0	1.77	14.07	0.88	2.95	0.11	1.21	0.8	–3.12
C	4.6	5.4	3.3	0.85	8.02	0.39	1.50	0.14	n.d.	1.0	
Profile S6 1660 m a.s.l.											
AE	4.2	4.9	49.3	6.69	13.05	8.57	8.14	0.95	6.19	6.7	2.61
Bs1	4.4	5.1	38.1	7.13	12.58	8.42	6.61	1.28	6.26	9.1	1.76
Bs2	4.6	5.2	16.6	5.53	9.70	8.80	4.60	2.14	5.13	15.2	1.79
BC	4.6	5.5	12.9	3.35	6.00	4.26	2.84	1.30	n.d.	9.2	
Profile S7 1995 m a.s.l.											
AE	4	4.8	85.9	8.33	12.17	7.28	9.34	0.62	5.60	4.4	2.82
BA	n.d.	5.1	64.5	n.d.	n.d.	n.d.	n.d.	n.d.	n.d.	n.d.	
Bs1	4.6	5.4	15.9	9.25	6.93	8.71	3.16	2.03	5.43	14.4	1.68
Bs2	4.8	5.4	8.7	7.57	7.35	8.17	2.80	2.23	3.23	15.8	2.31
BC	n.d.	5.3	3.8	n.d.	n.d.	n.d.	n.d.	n.d.	n.d.	n.d.	
C	4.8	5.6	3.0	2.88	2.47	2.58	0.78	0.78	n.d.	5.5	
Profile S8 2420 m a.s.l.											
OE	3.7	4.6	118.8	3.16	13.64	4.30	9.52	0.57	3.76	4.0	0.99
Bs	4.4	5.0	29.3	6.67	19.49	9.14	12.56	0.41	7.23	2.9	4.85
BC	4.5	5.1	7.8	4.41	12.47	4.59	4.20	0.49	n.d.	3.5	9.75

n.d. = not determined
[1]o = oxalate-extractable fraction, d = dithionite-extractable fraction, p = pyrophosphate-extractable fraction

TABLE 4. Geochemical characteristics (total contents) of the fine earth (<2 mm) and soil skeleton (2–200 mm) of the investigated soils.

Site and soil horizon	Depth (cm)	OM[1] (wt.%)	Al_2O_3 (wt.%)	SiO_2 (wt.%)	TiO_2 (wt.%)	CaO (wt.%)	MgO (wt.%)	K_2O (wt.%)	Na_2O (wt.%)	Fe_2O_3 (wt.%)	MnO_2 (wt.%)
North-facing sites											
Profile N1											
AE	4–10	2.47	15.36	62.65	0.73	1.10	1.17	2.21	1.76	5.11	0.08
Bs1	18–50	1.48	16.39	61.34	0.72	1.16	1.51	2.64	1.79	5.43	0.07
Bs2	50–90	0.30	17.26	62.20	0.67	0.79	1.12	2.99	1.67	5.66	0.06
BC	90–120	0.15	17.23	63.02	0.68	0.76	1.44	2.75	1.84	6.04	0.07
Profile N2											
E	6–12	6.67	11.55	65.26	0.92	1.01	1.33	1.73	1.08	4.47	0.12
Bs1	12–50	1.63	15.69	62.36	0.77	1.27	1.70	2.29	1.70	6.20	0.20
Bs2	50–100	0.54	15.78	62.09	0.78	1.86	2.34	2.26	1.89	6.60	0.62
C	130–150	0.19	15.57	67.65	0.63	1.45	1.99	2.34	2.32	5.13	0.20
Profile N3											
EA	1–10	33.37	11.51	37.49	0.59	0.59	0.58	1.65	0.92	3.56	0.04
Bhs	12–25	8.36	15.69	53.05	0.78	1.16	1.87	2.30	1.34	7.00	0.08
Bs	25–57	2.73	17.00	57.75	0.72	1.41	2.27	2.88	1.34	6.61	0.08
C	80–110	0.46	18.02	60.48	0.75	1.38	2.57	3.05	1.85	6.33	0.08
Profile N4											
OE	1–10	24.08	12.25	45.05	0.61	0.62	0.66	2.11	0.87	3.71	0.03
BE	10–35	5.21	14.46	61.09	0.71	1.03	1.64	1.93	1.49	2.65	0.06
Bhs	35–80	2.02	15.58	61.21	0.79	1.34	2.18	1.90	1.76	6.43	0.07
BC	80–100	0.68	17.59	59.63	0.78	1.19	2.31	2.16	2.05	6.28	0.06
BC/C mean[2]		0.38	17.17	62.62	0.67	1.10	1.98	2.58	2.06	5.93	0.10
s.d.[2]		0.22	0.94	3.13	0.10	0.34	0.47	0.35	0.22	0.48	0.06
South-facing sites											
Profile S5											
A	3–7	3.91	16.17	58.32	0.68	0.98	2.08	2.83	1.23	6.43	0.10
Bw1	7–20	1.64	16.12	62.44	0.81	0.89	1.94	3.12	1.39	6.45	0.11
Bw2	20–65	0.79	17.04	61.37	0.80	0.73	2.09	3.31	1.22	6.89	0.10
C	65–80	0.15	14.92	66.92	0.71	0.86	1.68	2.67	1.41	5.23	0.09
Profile S6											
AE	3–10	7.47	14.74	61.63	0.52	1.63	1.15	2.18	1.70	4.89	0.06
Bs1	10–50	5.41	14.72	64.07	0.51	1.72	1.17	2.54	1.77	4.18	0.06
Bs2	50–90	1.43	15.61	68.18	0.48	2.03	1.20	2.75	2.19	4.24	0.06
BC	90–125	0.68	15.57	67.80	0.70	2.25	1.62	2.84	2.15	5.03	0.07
Profile S7											
AE	0–10	14.69	12.38	56.86	0.35	1.74	1.10	2.43	1.27	3.97	0.06
Bs1	30–45	1.72	15.37	67.71	0.38	2.64	1.47	2.75	2.38	3.96	0.05
Bs2	45–70	1.01	15.15	67.37	0.38	3.08	2.59	2.48	2.41	4.44	0.06
C	95–110	0.30	14.18	69.83	0.36	2.67	3.35	2.67	2.37	3.94	0.06
Profile S8											
OE	2–6	20.31	12.49	49.56	0.72	1.06	1.58	2.17	1.45	5.17	0.08
Bs	6–35	3.24	15.71	56.94	0.80	1.31	2.11	2.07	1.71	7.05	0.11
BC	35–60	1.02	16.15	64.63	0.76	1.53	2.31	2.25	2.13	6.82	0.13
BC/C mean[2]		0.59	15.32	65.67	0.60	1.72	2.25	2.70	1.99	5.23	0.10
s.d.[2]		0.36	0.78	4.09	0.18	0.73	0.70	0.30	0.37	1.03	0.04

[1] Organic matter (of the fine earth and the soil skeleton) $\times 1.72$

[2] mean composition of the parent material (including standard deviation) of the north- and south-facing sites, respectively

TABLE 5. Minerals in the clay fraction of the investigated soil horizons: an overview.

Site	Horizon	Smec[1]	Verm[1]	Regular mica-smec	Regular mica-HIV or HIS	Irregular mica-HIV or HIS	Regular mica-verm	HIV[1]	HIS[1]	Chlorite	Mica	Kaolinite
N1	AE	x	x		x				x	(x)	x	x
EB		(x)		(x)			(x)	x	x	x	x	
Bs1							(x)	x	x	x	x	
Bs2					x		(x)	x	(x)	x	(x)	
BC					x		(x)		(x)	x	(x)	
N2	E	x	x	x		x			(x)		(x)	x
Bs1	?	(x)		x			x	x		(x)	x	
Bs2	?	(x)		x			x	x	(x)	(x)	x	
BC				x			x		x	x	(x)	
C				x			x		x	x	(x)	
N3	EA	x	x		x	x		?	(x)	(x)	x	x
E	x	x	(x)	x	x		(x)	x	(x)	x	x	
Bhs		(x)		x			(x)	x	x	x	x	
Bs				x			(x)	x	x	x	x	
BC				x			x		x	x	x	
C				x			x		x	x	x	
N4	OE	x	x	x			x				x	x
BE	x	x					(x)	(x)	(x)	x	x	
Bhs					x		(x)	x	x	x	(x)	
BC					x		x		x	x	(x)	
S5	A		(x)			x		x		(x)	x	x
Bw1					x		x		x	x	x	
Bw2					x		x		x	x	x	
C					x		(x)		x	x	x	
S6	AE		x			x		x	(x)	x	x	x
Bs1					x		x	(x)	x	x	x	
Bs2					x		x		x	x	x	
BC					x		x		x	x	x	
S7[2]	AE	(x)	x		x	x		x	(x)	x	x	x
BA		(x)			x		x	(x)	x	x	x	
Bs1					x		x		x	x	(x)	
Bs2					x		x		x	x	(x)	
BC					x		x		x	x	(x)	
C					x		(x)		x	x	(x)	
S8	OE	x	x		x			(x)	x	x	x	x
Bs		(x)			x		x	(x)	x	x	x	
BC					x		x		x	x	(x)	

x = present in significant amounts
(x) = traces
? = questionable, presence presumed
[1] HIV = hydroxy-interlayered vermiculite, HIS = hydroxy-interlayered smectite, verm = vermiculite, smec = smectite
[2] some amphibole and talc were present throughout the profile

1.02 nm, indicating the presence of HIV. The subsequent heat treatment at 550ºC did not noticeably change the XRD pattern, so that the peak around 1.1 nm was assigned to an irregularly-interstratified chlorite-HIV. The peaks at 2.43 (d_{001}*) and 1.27 (d_{002}*) could therefore represent

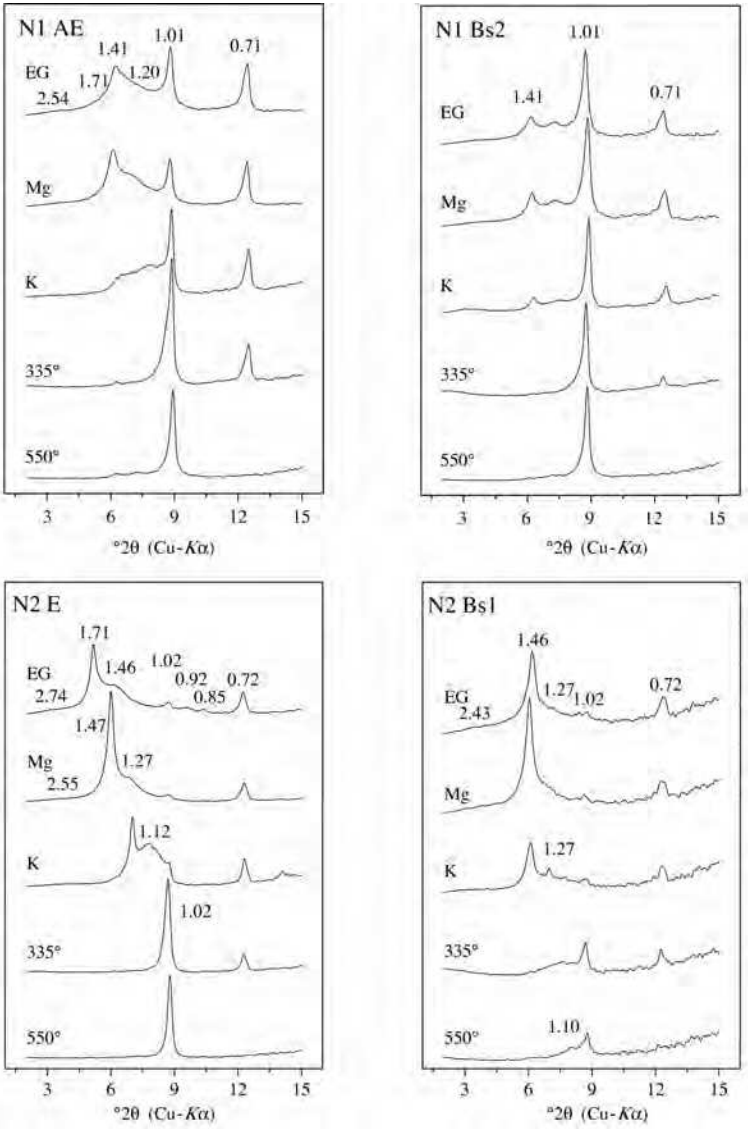

FIG. 2. XRD patterns of soil clays (<2 μm) of some selected horizons from the N1 and N2 north-facing soil profiles. The XRD curves were smoothed and corrected for Lorentz and polarization factors. *d* spacings are given in nm. EG = ethylene glycol solvation, Mg = Mg-saturation, K = K-saturation and corresponding heating treatments.

a regularly interstratified mica-HIV (Mg-saturation or EG-solvation, see Fig. 2). Kaolinite was identified by the peak at 0.72 nm. No chlorite was detected. The clay mineralogy of the Bs2 horizon sample was similar to that of the previously described horizon, except for the appearance of a small amount of chlorite. Furthermore, HIV and chlorite-HIV showed a greater resistance to collapse with the heating process. The clay sample from the BC horizon contained more mica. Also, regularly interstratified mica-HIV and hydroxy-interlayered vermiculite were detected, together with chlorite and kaolinite. The clay mineralogy of the sample from the C horizon was similar to that of the BC horizon.

The EG-solvated sample from the EA horizon of soil profile N3 at 1930 m a.s.l. showed seven peaks centred at 2.43, 1.70, 1.44, 1.24, 1.07, 1.01 and

0.72 nm (Fig. 3). The peak at 1.44 nm partly collapsed to 1.01 after K-saturation and further after heating at 335ºC. A very small 1.44 nm peak persisted even after heating at 550ºC; therefore vermiculite, HIV and chlorite were identified. The peak at 1.24 nm shifted towards 1.01 nm after K-saturation and heating at 335ºC, and collapsed following heating at 550ºC. This peak was attributed to a regularly-interstratified mica-HIV, whose d_{001}* reflection was detected at 2.43 nm (together with the d_{002}* peak at 1.24 nm). The peak at 1.07 nm had a similar behaviour and could be

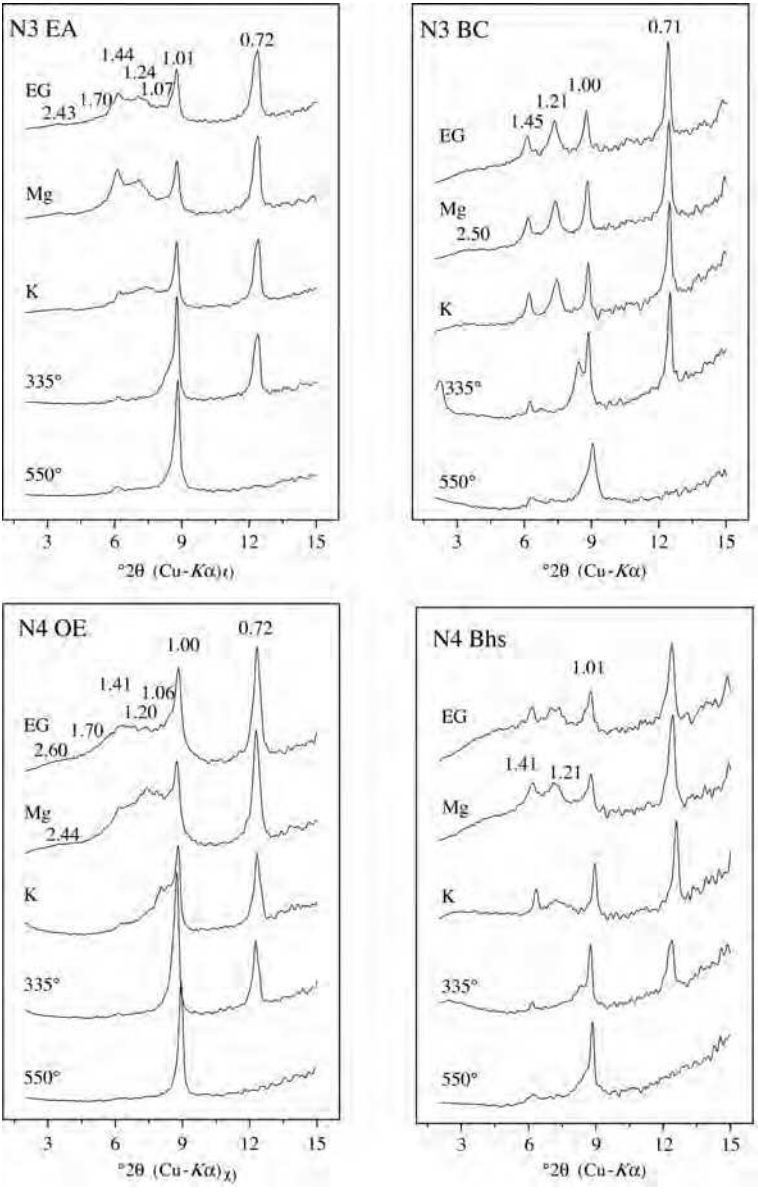

FIG. 3. XRD patterns of soil clays (<2 μm) of some selected horizons from the N3 and N4 north-facing soil profiles. The XRD curves were smoothed and corrected for Lorentz and polarization factors. *d* spacings are given in nm. EG = ethylene glycol solvation, Mg = Mg-saturation, K = K-saturation and corresponding heating treatments.

assigned to an irregularly-interstratified mica-HIV. Kaolinite was also present in this horizon (Fig. 3). The E horizon exhibited the same minerals as the EA horizon (data not shown), with a higher content of mica and a smaller degree of polymerization within the vermiculitic components. An expandable mineral with a *d* spacing of 1.56 nm in the EG-solvated sample indicated some interstratification of smectite with a high-charged component (smectite-vermiculite). The XRD pattern of the EG-solvated sample of the Bhs horizon showed an increased intensity of the peak at 1.25 nm, belonging to a regularly interstratified mica-HIV (data not shown). The peaks at 1.44 and 1.24 nm (Mg-saturation) showed a slightly higher resistance to collapse following K-saturation and heating at 335ºC. A small amount of chlorite (peak persisting at 1.44 nm after heating) and kaolinite (0.72 nm) were also identified. The mineralogy of the Bs horizon was identical to that of the Bhs horizon. The mineralogy of the BC (Fig. 3) and C horizons was different from that of the previous horizon, with a higher intensity of the peak at 1.21 nm and a lower intensity of the peak at 1.45 nm. Saturation with K did not cause any difference to the Mg-saturated sample, while heating distinctly increased the peak intensity near 1.01 nm. Together with the peak at 2.50 nm (Mg-saturation), a regularly-interstratified mica-HIV (with d_{001}* at 2.50 nm and d_{002}* at 1.21 nm) could be identified.

An XRD pattern of the Mg-saturated sample from the OE horizon of soil profile N4 at 2390 m a.s.l. showed peaks at 2.44, 1.41, 1.20, 1.06, 1.00 and 0.72 nm. EG-solvation caused the expansion to 1.70 nm of the peak at 1.41 nm, indicating the presence of smectite (Fig. 3). Furthermore, a portion of the peak at 1.20 nm expanded to 1.41 nm, whereas the peak at 1.06 nm maintained its position. The subsequent K-saturation and heating at 335ºC revealed the presence of vermiculite, a regularly-interstratified mica-smectite and interstratified mica-vermiculite minerals. A major proportion of mica and kaolinite was also identified in this sample (Fig. 3). The XRD pattern of the EG-solvated sample from the BE horizon (data not shown) showed the presence of smectite and partly hydroxy-interlayered vermiculite. Mica, kaolinite and traces of chlorite were also observed. The sample from the Bhs horizon exhibited a relatively small amount of mica (peak at 1.01 nm, Mg-saturated sample) compared to the other 2:1 phyllosilicates. HIV, mica-HIV, kaolinite and chlorite were also identified, whereas no smectite or vermiculite was detected in this horizon (Fig. 3). The clay mineralogy of the BC horizon was similar to that of the Bhs horizon. The mica seemed more weathered, as shown by a broad peak at 1.01 nm, and also present in a smaller amount. A minor amount of chlorite was also detected.

South sequence. The surface A horizon of soil profile S5 at 1200 m a.s.l. showed an intense mica peak at 1.00 nm in the XRD pattern of the EG-solvated sample (Fig. 4). The presence of kaolinite was indicated by a peak at 0.71 nm and confirmed by FTIR. A less intense peak at 1.40 nm remained unaffected after K-saturation. Although most of this peak collapsed to 1.00 nm at 335ºC, a very small part remained following heating at 550ºC, indicating the presence of HIV and traces of chlorite. A small peak at 1.19 nm was attributed to an irregularly-interstratified mica-HIV that collapsed to 1.00 nm after heating at 550ºC (Fig. 4). The mineralogies of the lower Bw1, Bw2 and C horizons were similar to that of the A horizon.

The EG-solvated clay sample from the AE horizon of soil profile S6 showed a very intense peak at 1.42 nm, a kaolinite peak at 0.71 nm, a minor mica peak at 1.00 nm and two peaks at 1.21 and 1.04 nm (Fig. 4). The peaks at 1.42, 1.21 and 1.04 nm shifted towards 1.00 nm after treatment at 335ºC, but two peaks at 1.42 and around 1.21 nm persisted even after heating the sample at 550ºC (Fig. 4). This indicated the presence of irregularly-interstratified mica-HIV and chlorite-HIV. The sample from the Bs1 soil horizon showed a very similar XRD pattern, whereas the lower horizons Bs2 (Fig. 4) and BC horizons, although containing the same clay minerals, had a smaller amount of HIV and a larger proportion of mica.

The clay mineral composition of the S7 soil profile at 1995 m a.s.l. was similar to that of the S5 and S6 soil profiles. At best traces of smectite were detected in the AE surface horizons (some interstratified smectite with vermiculite, detectable around 1.5 nm). The XRD peaks of the EG-solvated sample at 2.48, 1.42, 1.22, 1.10, 1.01, 0.94 and 0.72 nm (Fig. 5) allowed the identification of vermiculite (mostly hydroxy-interlayered), HIV, regularly-interstratified mica-vermiculite (with a d_{001}* and d_{002}* at 2.48 and 1.22 nm, respectively), mica, chlorite and kaolinite. Some talc was identified by a peak at 0.94 nm. The same minerals were detected in the lower BA, Bs1, Bs2, BC and C horizons, with vermiculite progressively disappearing and HIV and

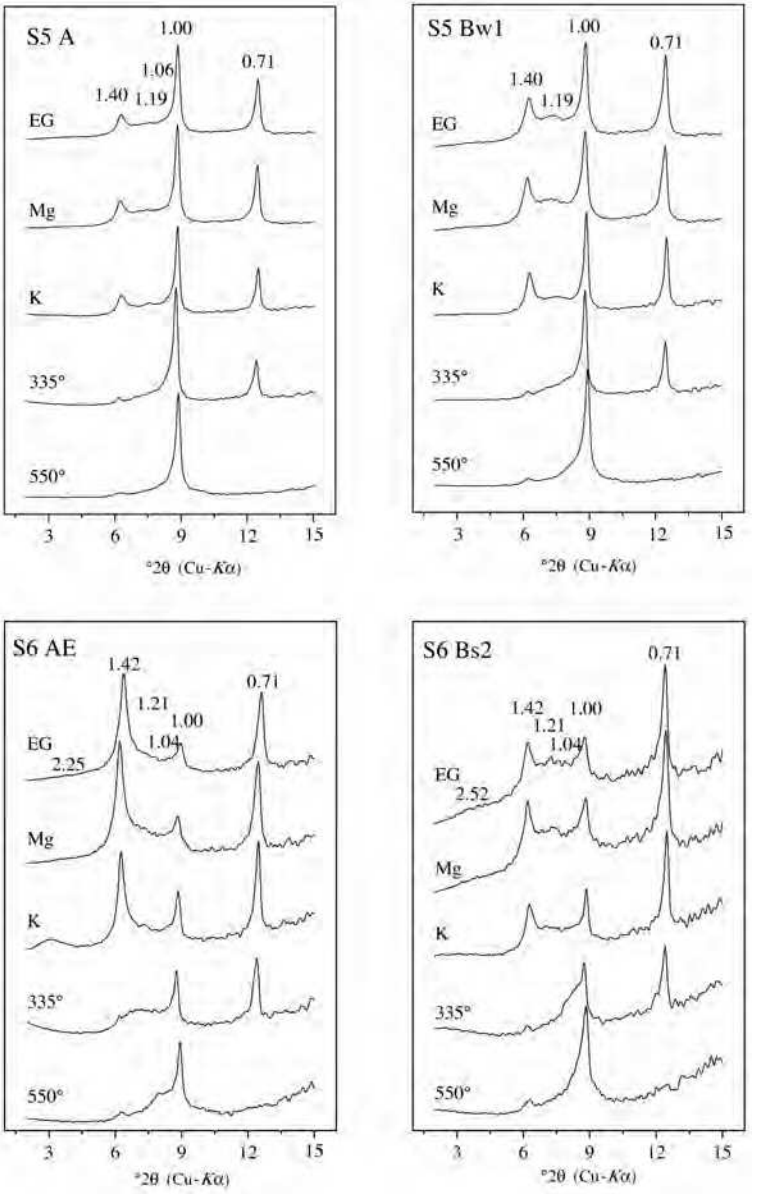

FIG. 4. XRD patterns of soil clays (<2 μm) of some selected horizons from the S5 and S6 south-facing soil profiles. The XRD curves were smoothed and corrected for Lorentz and polarization factors. *d* spacings are given in nm. EG = ethylene glycol solvation, Mg = Mg-saturation, K = K-saturation and corresponding heating treatments.

regularly-interstratified mica-HIV decreasing in favour of mica and chlorite with depth.

Peak decomposition allowed the separation of XRD peaks at 2.52, 1.64, 1.43, 1.23, 1.04, 1.00 and 0.72 nm (Fig. 5) in the EG-solvated clay sample from the OE horizon of soil profile S8. Smectite could therefore be identified by the peak at 1.64 nm. Vermiculite, regularly interstratified mica-HIV (on the basis of the d_{001}* and d_{002}* at 2.52 and 1.23 nm) and irregularly-interstratified mica-HIV, chlorite, mica and kaolinite could be identified with the K-saturation and heating

treatments at 335 and 550ºC (Fig. 5). Except for the absence of a peak near 1.64 nm, the mineralogy of the lower horizon Bs was similar both in the typology and peak intensities to that of the surface OE horizon. The BC horizon showed the same clay minerals (Fig. 5), but differed from the previous horizons by a higher amount of interstratified mica-HIV and a slightly higher resistance of HIV and mica-HIV minerals to collapse to 1.0 nm following the heat treatment at 335ºC (Fig. 5).

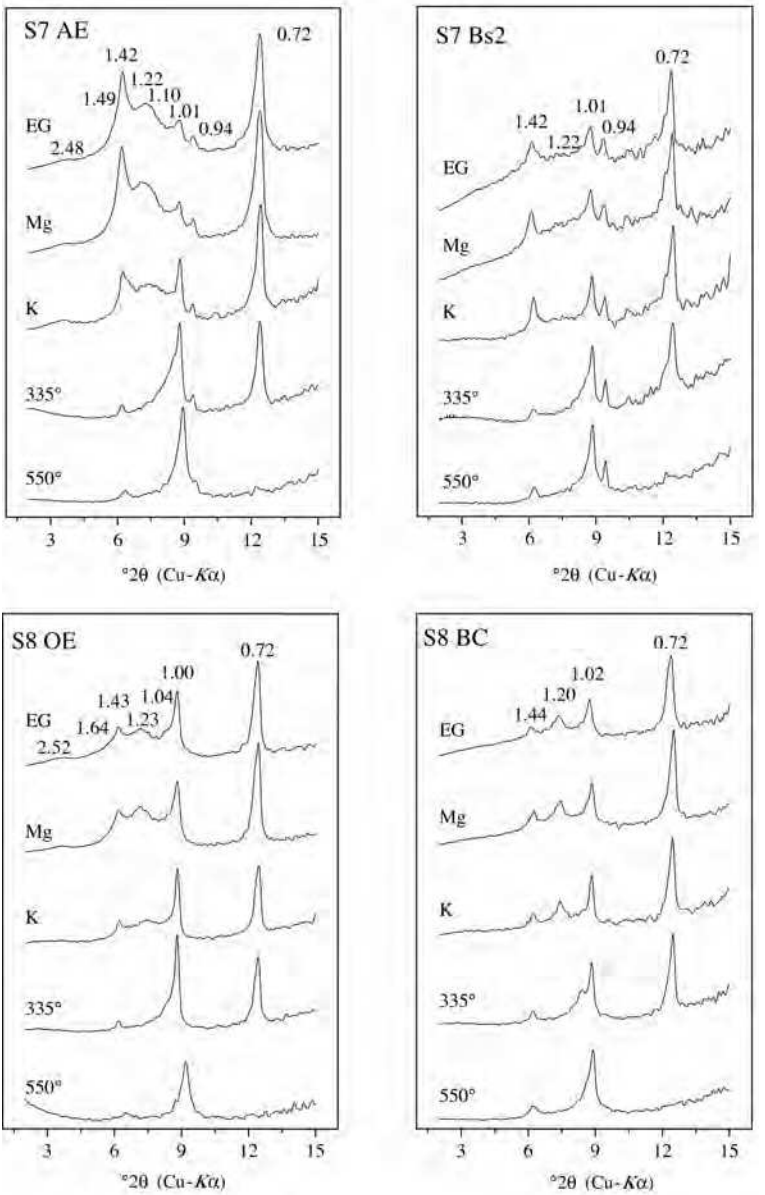

FIG. 5. XRD patterns of soil clays (<2 μm) of some selected horizons from the S7 and S8 south-facing soil profiles. The XRD curves were smoothed and corrected for Lorentz and polarization factors. *d* spacings are given in nm. EG = ethylene glycol solvation, Mg = Mg-saturation, K = K-saturation and corresponding heating treatments.

Citrate treatment of the clay fraction

Hydroxy interlayers hinder the collapse of expandable 2:1 phyllosilicates when K-saturated, and the expansion of low-charge expandable minerals when EG-solvated (Karathanasis, 1988; Barnhisel & Bertsch, 1989). Citrate treatment was effective in removing the hydroxy interlayers from 2:1 phyllosilicates in the north-facing soils. In the surface AE horizon of the soil profile N1, a well defined peak was present around 1.61 nm (Fig. 6). The slightly smaller value of the *d* spacing of this expandable mineral could indicate some interstratification between a high- and a low-charge component. In the lower horizons no smectite was detected, but a full collapse to 1.0 nm of the peaks at 1.43 nm was obtained following K-saturation (data not shown).

The EG-solvated sample from the E horizon of soil profile N2 displayed a very intense peak at 1.67 nm, whereas no peak was present in the region of 1.27 nm (Fig. 6). This points to the presence of some irregularly-interstratified mica-HIS, the expansion of this mineral following EG-solvation having been hampered by the hydroxy interlayers. Smectite was also detected in the lower Bs1 and Bs2 horizons, while it was absent in the lowest BC and C horizons. K-saturation caused a full collapse to 1.0 nm of the 2:1 expandable phyllosilicates.

Smectite (interstratified with some vermiculite) was identified in the surface EA horizon of soil profile N3 by a subordinate peak at 1.56 nm in the EG-solvated sample (Fig. 6), while an irregularly-interstratified smectite-vermiculite component was observed in the lower E horizon. Collapse of the 2:1 expandable component to 1.0 nm was achieved with K-saturation in all the horizons.

Smectite was present in the OE (Fig. 6) and BE surface horizons of soil profile N4, while collapse to 1.0 nm of the peaks at 1.43 and 1.25 nm was obtained following K-saturation, with the exception of a minor chlorite peak.

No smectite was detected in the surface horizons of the south-facing soils S5 and S6. Smectite was observed in the surface OE horizon of the soil profile S8, while a smectitic component showing a certain degree of interstratification – due to its position at 1.58 nm following ethylene glycol-solvation – was found in the surface horizon of the soil profile S7 (Fig. 7). The citrate treatment was effective in removing the hydroxy interlayers from 2:1 expandable phyllosilicates that collapsed to 1.0 nm following K-saturation.

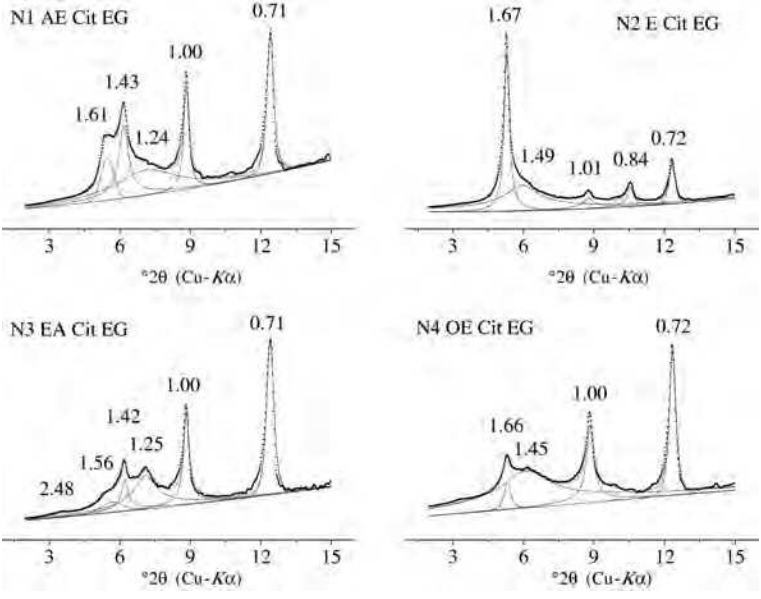

FIG. 6. XRD patterns of the Na-citrate-treated and ethylene glycol(EG)-solvated soil clays (<2 μm) from the surface horizon of the north-facing soil profiles. The XRD curves were corrected for Lorentz and polarization factors. *d* spacings are given in nm.

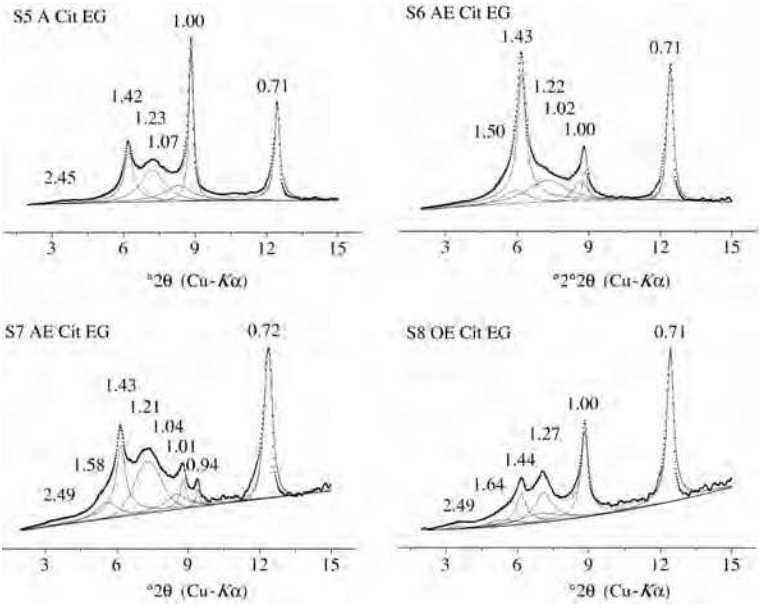

FIG. 7. XRD patterns of the Na-citrate treated and EG-solvated soil clays (<2 μm) from the surface horizon of the south-facing soil profiles. The XRD curves were corrected for Lorentz and polarization factors. *d* spacings are given in nm.

Figure 8 shows FTIR spectra of the clay samples from the N2 E and S5 A horizons before and after Na-citrate treatment. Various regions in the IR spectrum contain OH vibrational information. In the OH-bending region, the bands associated with hydroxyl groups can be discriminated from each other, and band assignment is straightforward. Furthermore, this region is not affected by the presence of residual water molecules (Vantelon *et al*., 2001). For the south-facing site, there are no differences detectable before and after the hot citrate treatment. The IR spectra of the north-facing site, however, showed some small changes, especially in the region between 830 cm^{-1} to 750 cm^{-1}. The band at 830 cm^{-1} can be attributed to δ_{AlMgOH} (Farmer, 1974) and that at 799 cm^{-1} to Si−O−Al bands (and quartz together with the doublet at 779 cm^{-1}). Some changes can be seen in the region of 820 cm^{-1} and 790 cm^{-1}. The band at 820 cm^{-1} can be assigned to δ_{FeFeOH} (Farmer, 1974; Goodman *et al*., 1976) and the region near 786 cm^{-1} to δ_{FeMgOH} (Vantelon *et al*., 2001). The decrease in these bands of the samples from the north-facing site after the hot citrate treatment may point to the better dissolution of octahedral Al- and Mg-interlayers of clay minerals when compared to the south-facing site. The citrate treatment was probably less effective for the samples from the south-facing site, where some residual Al still remained in the interlayers. The absorption band at 690 cm^{-1} points to dioctahedral smectites. According to Bishop *et al*. (2002), smectites with a high proportion of tetrahedral Fe^{3+} display a strong band near 680 cm^{-1}. In the measured samples, some Fe^{3+} seems therefore to be present in the structure of smectite-like minerals. No significant differences in the intensity of this band before and after the treatment were measurable.

Thermogravimetric (TG) analysis records the weight changes of a sample during dynamic heating. Using derivative thermogravimetric analysis (DTG), it is possible to distinguish between overlapping reactions that might be difficult to discern with TG data alone. Thermogravimetric analyses indicated the presence of adsorbed water (up to temperatures of 120ºC) and water from interlayers (especially discernible in the temperature range of 100−250ºC) in all samples measured (Fig. 9). After citrate treatment, the amount of adsorbed water was generally lower due to the destruction (chelation) of organic matter. The clay samples of the site N2 (E-horizon) showed pronounced peaks at 70ºC (adsorbed water) and at 190ºC (water from interlayers). The sample of the south-facing site

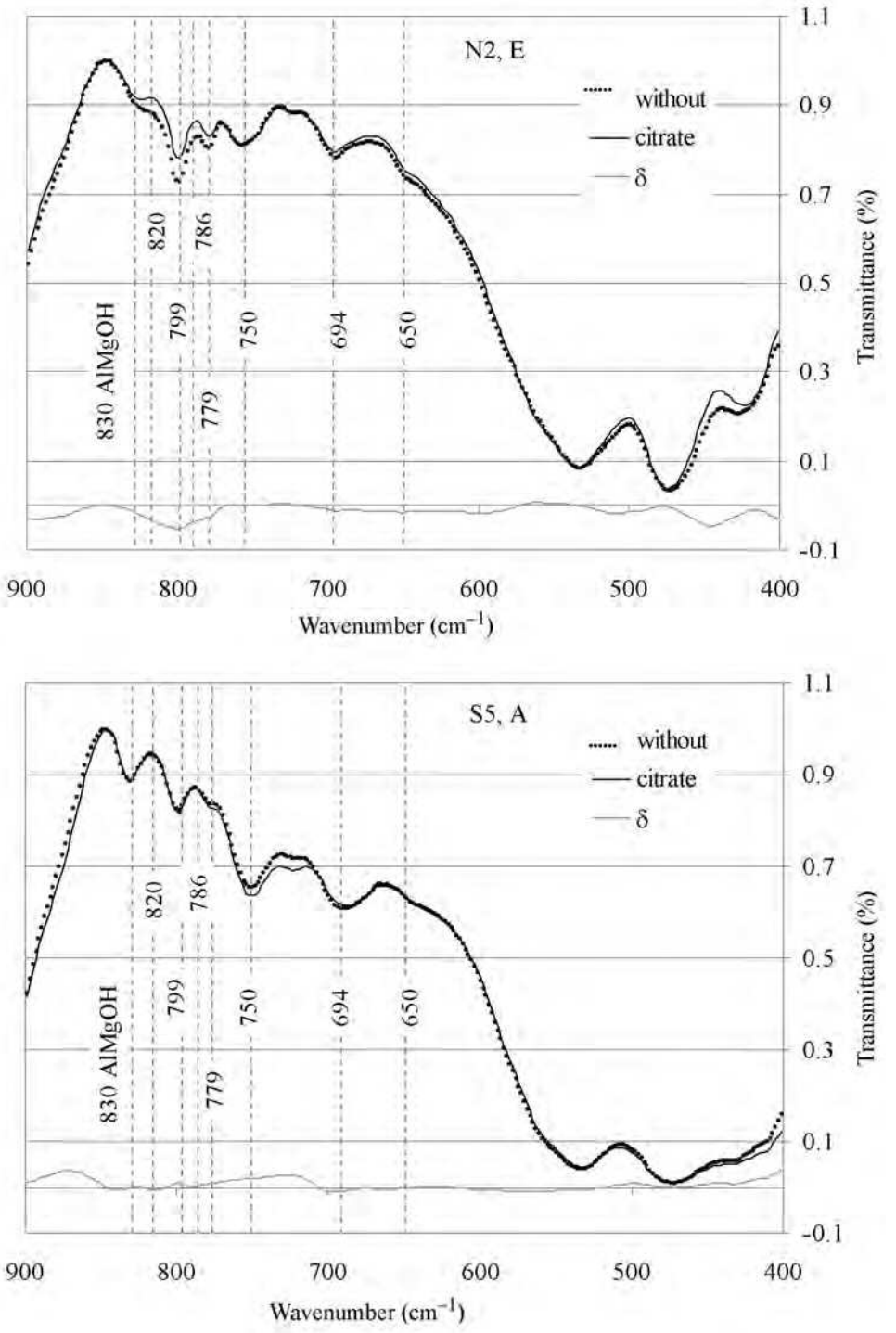

FIG. 8. Comparison of FTIR spectra in the OH bending and $M-O$ region (900 to 300 cm^{-1}) between untreated soil clay samples and hot Na-citrate-treated samples of a north- and south-facing site (N2: north-facing, 1620 m.a.s.l., E horizon; S5: south-facing, 1185 m a.s.l., A horizon).

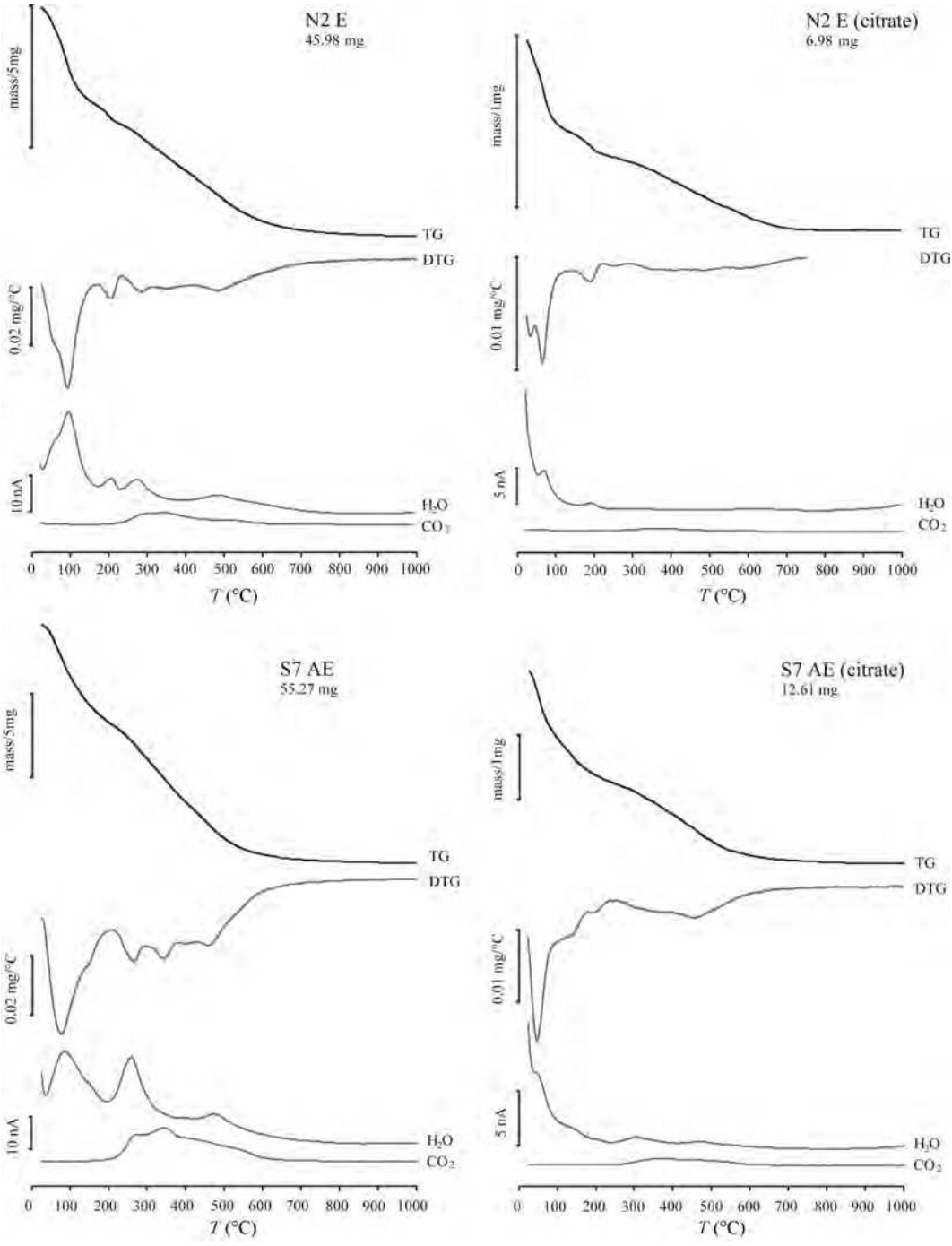

FIG. 9. Thermogravimetric analyses of typical topsoil samples (north- and south-facing sites) before and after citrate treatment.

(S7, AE horizon) had a distinct peak at 50ºC (adsorbed water) and minor peaks at 150 and 200ºC (water from interlayers). These analyses confirm the presence of clay minerals with H_2O-interlayers on both south- and north-facing sites.

Trioctahedral vs. dioctahedral transformation

The XRD patterns in the d_{060} region are shown in Fig. 10. At the lowest site in the north sequence, only small differences within the soil profile could

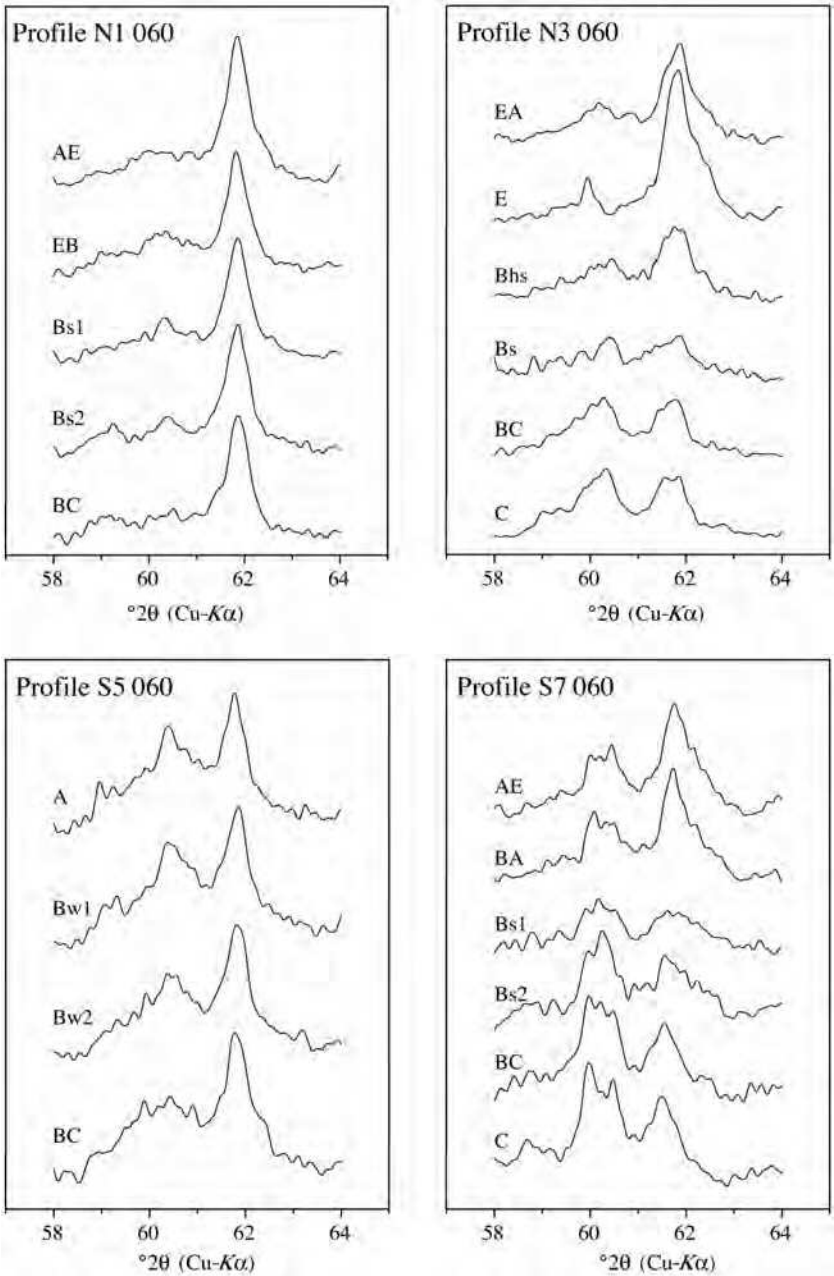

FIG. 10. XRD patterns in the d_{060} region of the soil clays from all the horizons of the N1 and N3 north-facing and S5 and S7 south-facing soil profiles.

be detected. Major changes were measurable in the N2, N3 and N4 soil profiles, with trioctahedral species, represented by peaks in the range 59−61°2θ, decreasing from the lowest horizons towards the top of the soil profile, and correspondingly, dioctahedral species increasing, in the range 61−63°2θ. The highest proportion of trioctahedral species was measured in the lowest C horizon of N3 soil profile (Fig. 10).

On the south-facing slope no differences could be detected in the samples from the soil profile S5 (Fig. 10), whereas trioctahedral species decreased and dioctahedral species increased distinctly upwards in the soil profiles S6 and S7 (Fig. 10). A similar trend, but less pronounced, could also be observed in the soil profile S8.

Layer charge estimation

In general, long-chain alkylammonium C_{18} and C_{12} complexes showed well developed low-charge phyllosilicates with a total layer-charge value per half unit cell (ξ) ranging from 0.22 to 0.30 in the surface horizons of the north-facing soils (Fig. 11). The low charges are due to pedogenetic processes and partially inherited from the parent material (see below).

Low-charge clay minerals were also detected in the surface horizons of the south-facing soils, more obviously in soil profiles S7 and S8, developing at 1995 and 2420 m a.s.l., respectively, and, to a lesser extent, in the soil profile S6 at 1660 m a.s.l. The intensity of the low-charge clay mineral peak was quite low in the soil profile S5 (Fig. 11). The total layer-charge value per half unit cell (ξ) for the soils on south-facing slopes ranged between 0.29 and 0.30.

These results are in agreement with the analyses carried out in the d_{060} region, where the samples from the south-facing soils showed a transformation from trioctahedral to dioctahedral species. Iron oxidation and the substitution of Fe^{3+} and/or Al^{3+} for Mg^{2+} contributed to the decrease of phyllosilicate charge (Carnicelli *et al*., 1997). The failure of ethylene glycol solvation to expand low-charge phyllosilicates following the hot citrate treatment may be due to the presence of residual hydroxy-polymers in the interlayers of 2:1 phyllosilicates that hindered the access of organic molecules.

DISCUSSION

Soils developing on the north- and south-facing slopes showed a coarse texture and a low pH. These

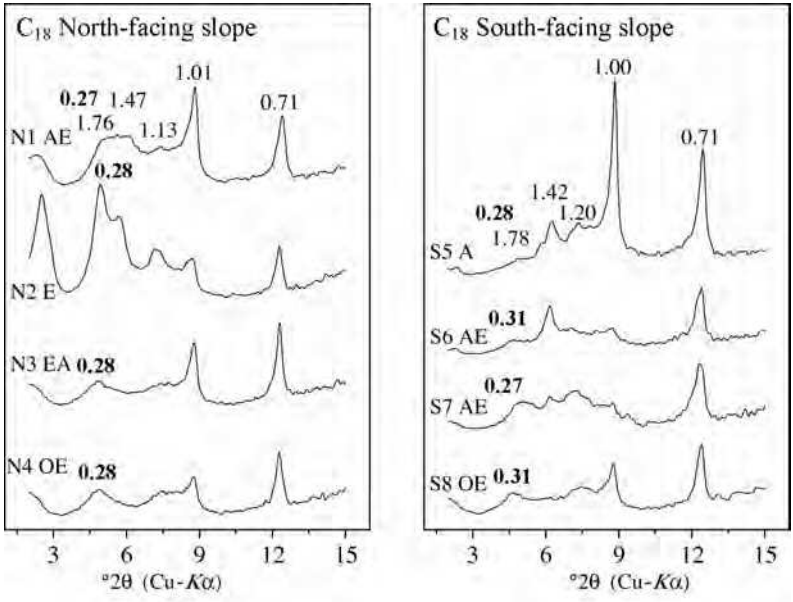

FIG. 11. XRD patterns of soil clays (<2 μm) from the surface horizons of the north- and south-facing soil profiles. Clays were treated with C_{18} alkylammonium ions. The XRD curves were corrected for Lorentz and polarization factors. *d* spacings are given in nm. The bold numbers indicate the calculated layer charge per half unit cell.

features are paramount for the development of podzols (De Coninck, 1980).

Generally, the podzolization process (i.e. eluviation and illuviation of Fe, Al and partially organic C) was more intense on soils developing on the north-facing slopes (Table 6). The concentrations of secondary Fe- and Al-forms in the B horizon were in most cases greater at the north-facing sites. In this particular environmental setting, Fe and Al are continuously released, mostly from primary minerals (but probably also from secondary Fe and Al phases) by the intense weathering (as indicated by the high Fe_o/Fe_d-ratio). The transfer of Fe and Al within the soil profile is primarily thought to occur as metal-organic complexes (or partially, for Al, as aquo-ion). Smaller amounts of organic complexing agents at south-facing sites were probably exposed to the relentless supply of metal cations liberated by weathering. The total amount of organic matter in the mineral soil (data not shown) is similar at both north- and south-facing sequences. More organic ligands have probably been available at the north-facing sites, leading to more intense weathering and higher eluviation. More ligands could have been supplied by the wetter soil conditions (see below) and/or also by slightly differing vegetation.

TABLE 6. Comparison of data related to eluviation, illuviation, acidification and ITM between north and south slopes.

Variable	North slopes mean (s.d.)	South slopes mean (s.d.)
E or A horizon		
Al_o (g/kg) [1)]	4.77 (3.30)	5.33 (3.30)
Fe_o (g/kg)	8.16 (2.75)	7.56 (2.95)
Si_o (g/kg)	0.33 (0.43)	0.61 (0.27)
ITM (%)[2)]	0.17 (0.34)	0.10 (0.20)
Al_d (g/kg)	4.19 (3.00)	5.03 (2.98)
Fe_d (g/kg)	18.51 (4.00)	14.04 (2.25)
pH ($CaCl_2$)	3.48 (0.37)	4.08 (0.30)
Uppermost B horizon		
Al_o (g/kg)	7.92 (4.37)	6.90 (3.73)
Fe_o (g/kg)	13.53 (6.28)	6.50 (4.31)
Si_o (g/kg)	0.58 (0.41)	0.97 (0.85)
ITM (%)	n.d.	0.73 (0.60)
Al_d (g/kg)	8.18 (4.71)	6.35 (2.90)
Fe_d (g/kg)	30.42 (8.50)	14.81 (6.28)
pH $CaCl_2$)	4.08 (0.10)	4.35 (0.25)
Second B horizon		
Al_o (g/kg)	9.61 (4.96)	5.61 (3.66)
Fe_o (g/kg)	11.93 (4.20)	3.64 (0.90)
Si_o (g/kg)	1.45 (1.31)	1.24 (1.10)
ITM (%)	1.03 (0.93)	0.78 (0.78)
Al_d (g/kg)	9.25 (5.11)	4.57 (2.52)
Fe_d (g/kg)	30.38 (8.28)	10.90 (2.98)
pH ($CaCl_2$)	4.38 (0.15)	4.45 (0.39)

[1] o = oxalate extractable content, d = dithionite extractable content
[2] only values considered where ITM is probable (molar ratio of $(Al_o - Al_p)/Si_o$ between 0.75 and 2.4).
n.d. = not detectable

The degree of chemical weathering increased from the south-facing sites, that have more favourable thermal conditions, to the north-facing sites, which are characterized by lower temperatures, lower evapotranspiration and higher humidity (cf. Hunckler & Schaetzl, 1997). Due to the abundant precipitation, water should not be a limiting factor, and thus weathering should be enhanced in Alpine regions having higher temperatures. Water nevertheless also seems to be a determining factor in Alpine regions. During winter, the snowpack may affect pedogenesis and podzolization. Thick snowpack inhibits or reduces soil frost and allows large fluxes of snowmelt water to infiltrate into already moist profiles (cf. Schaetzl & Isard, 1996). This type of flux (slow, steady, cold water) may be particularly effective in enhancing the podzolization process. A reduced snow cover, higher evapotranspiration rates and reduced water fluxes (especially during snowmelt in spring) are expected on south-facing sites. Soil-mapping studies (Sartori *et al*., 2005) carried out in these Alpine regions came to similar conclusions, that soils generally showed signs of more intensive weathering processes on north-facing sites.

As a consequence of the greater weathering intensities on the north-facing slope, a greater amount of smectite was measured in the surface horizon of the profile N2 located at 1660 m a.s.l., in the sub-alpine belt. Smectite was also detected in soils N3 and N4, developing, on the same slope, at 1910 and 2390 m a.s.l. These results are in agreement with those obtained in similar Italian Alpine environments (Mirabella & Egli, 2003; Egli *et al*., 2003b, 2004). The formation of smectite depends principally on the presence of complexing organic compounds that are able to remove hydroxy-polymers from the interlayers of 2:1 low-charge expandable minerals (Lundström *et al*., 2000; Mirabella & Egli, 2003). On the south-facing slope, smectite was found only in the surface

horizon of soil profile S8, located at 2420 m a.s.l. Climatic conditions suitable for the development of podzols are therefore found at a higher altitude on the south-facing slopes compared to the north-facing slopes. These results are in agreement with the degree of podzolization that was found to be significantly greater on N-NE facing slopes in Baraga County, Michigan, as compared to S–SW facing slopes (Hunkler & Schaetzl, 1997).

The citrate treatment allows the removal of hydroxy-polymers which are not too strongly bound to 2:1 clay-sized phyllosilicates within their interlayer space. Subsequent XRD determinations may reveal the presence of low-charge clay minerals the expansion of which, following ethylene glycol solvation, was hindered by the interlayered polymers (Karathanasis, 1988). Furthermore, when saturated with K (Barnhisel & Bertsch, 1989), hydroxy-polymers prevent the collapse of the 2:1 expandable phyllosilicates to a mica-like structure. In soils with north exposure, citrate effectively extracted the hydroxy-interlayered polymers. In the surface horizon of soil profile N1 (1200 m a.s.l.), smectite – exhibiting a certain degree of interstratification for its *d* spacing at 1.61 nm – could be identified, whereas all 1.4 nm structures collapsed to 1.0 nm following K-saturation. Smectitic compounds could also be identified in the lower B horizons of the soil profiles N2, N3 and N4. This indicated that low-charge clay minerals were already present in the deeper horizons of these soils, but their identification had not been possible because of the interference of hydroxy-polymers. Similar results have previously been reported in a climosequence of soils developing on granite in a north-facing slope in Trentino (Mirabella & Egli, 2003).

The same procedure applied to soils with south exposure showed different results. After the hot citrate treatment and the ethylene glycol-solvation, no or only weak (surface horizons of S8 and S7) expansions of 2:1 phyllosilicates were observed. The collapse of these minerals to 1.0 nm following K-saturation was very evident. Theoretically, this should indicate that 2:1 clay phyllosilicates had no substitution of trioctahedral cations (Mg^{2+}, Fe^{2+}) by dioctahedral ones (Al^{3+} and Fe^{3+}). The XRD analysis of the d_{060} region and the determination of layer charge of clay minerals by the long-chain alkylammonium ion C_{18} and C_{12}, however, did not fully confirm the absence of such a process. Transformation from trioctahedral to dioctahedral species was, in fact, also detected in the south-facing soils, though less evident than on the north-facing sites. In agreement with these results, some low-charge clay minerals (ξ ~0.30) were detected in the surface horizons of soils from the south sequence, especially in soil profiles S7 and S8. Layer charge was also checked by the long-chain alkylammonium C_{12} (results not shown), and the results were similar to those obtained with the C_{18} chain.

The failure of EG to expand the low-charge phyllosilicates after the removal of hydroxy-polymers could be due to the presence of residual hydroxides in the interlayers of the mineral structures that hindered access to the organic molecules. The smaller K^+ cation was, however, able to enter into the interlayer space of 2:1 expandable clay-sized phyllosilicates and to expel the polymers, causing the collapse of the mineral structure.

Our results have confirmed that podzolization processes, as regards the removal of hydroxy-polymers and their eluviation in the soil profile, are most intense in the range of the sub-alpine forest up to the timberline (1600–1900 m a.s.l.) in soils with north exposure. Although Alpine regions exhibit an overall abundant precipitation, the actual availability of water and consequently water-flows in the soil play a decisive role in the weathering, leaching of elements and organic compounds, and in the transformation of (clay) minerals (cf. Dambrine, 1986; Schaetzl & Isard, 1996; Muhs *et al*., 2001; Hall *et al*., 2002). We hypothesise that the formation of smectites (with a low charge and dioctahedral structures) as a weathering end-product has been enhanced at the north-facing sites due to reduced evapotranspiration and consequently a greater soil moisture. Favoured by the presence of low molecular weight acids (van Hees *et al*., 2000), leaching of elements and weathering conditions was enhanced.

In particular, the reduction of the charge of clay minerals also took place in those horizons where hydroxy-polymers hinder the detection of expandable minerals with ethylene glycol- or glycerol-solvation procedures (Karathanasis, 1988; Barnhisel & Bertsch, 1989). Due to the more intense podzolization process near the timberline, vermiculites and smectites in the surface soil horizons of the north sequence usually contained no or only a small amount of hydroxy interlayers. At the south slope, hydroxy interlayering was consequently more pronounced (some of these interlayers were even

not removable with citrate). The site at the lowest altitude and with the lowest susceptibility to weathering consequently had the largest amount of HIV(HIS) or interstratified mica-HIV(HIS). The charge reduction of smectite precursor clay minerals, such as mica and chlorite, also took place in the Bhs and Bs horizons, where smectitic phases were predominantly hydroxy-interlayered. The reduction of the charge of 2:1 phyllosilicates therefore occurred before the removal of hydroxy-polymers by fulvic acids and low molecular weight organic acids. This was indicated in part by the citrate treatment, where a greater proportion of 2:1 minerals expanded after EG solvation, but mainly by the detection of the transformation of trioctahedral into dioctahedral species and by the alkylammonium procedure.

CONCLUSIONS

In earlier investigations, weathering in cold regions was usually focused on the notion of 'cold', such that chemical processes are temperature-inhibited, often to the point of non-existence (cf. Hall *et al*., 2002). Works by Reynolds (1971), Anderson *et al*. (1997), Allen *et al*. (2001) and others are examples attesting to the potentially advanced nature of chemical weathering and mineral transformations in glaciated mountains. We give evidence in this investigation that weathering and mineral transformation or formation can be intense in sub-alpine and alpine belts, and therefore cold environments. It is shown that weathering and mineral formation and transformation is not primarily temperature-inhibited, but could conceivably be limited by moisture availability. The two soil sequences revealed different degrees of podzolization, with more advanced stages in the north-facing soils, especially those developing near the timberline. The process leading to the formation of smectite in the north sequence was the result of the removal of hydroxy polymers from the interlayer of low-charge expandable phyllosilicates. This process is generally favoured by the presence of easily-chelating organic compounds, mainly fulvic and low molecular organic acids, and the availability of water.

Besides the eluviation process, clay minerals underwent a process of ionic substitution in the octahedral sheet that led to a decrease of the layer charge. The charge reduction was also detectable in the soils of the south sequence, but in a narrower altitude range (from 2000 to 2400 m a.s.l., when compared to the range of 1660–2400 m a.s.l. found for the north sequence soils).

This process could not be detected by standard XRD determination, because of the presence of interlayered hydroxy-polymers that hinder the access of ethylene glycol molecules into the interlayer spaces of the minerals. Hydroxy interlayering was more evident in the south sequence, and the hot citrate treatment only partially removed the Al polymers.

ACKNOWLEDGMENTS

This research was partially supported by a grant from the Ministero delle Politiche Agricole e Forestali (Roma, Italia; project: MEPESA). We would like to express our appreciation to Dr A. Campbell, to an unknown reviewer and to Dr E. Murad for their helpful comments on an earlier version of the manuscript

REFERENCES

Allen C.E., Darmody R.G., Thorn C.E., Dixon J.C. & Schlyter P. (2001) Clay mineralogy, chemical weathering and landscape evolution in Artic-Alpine Sweden. *Geoderma*, **99**, 277–294.

Anderson H.A., Berrow M.L., Farmer V.C., Hepburn A., Russell J.D. & Walker A.D. (1982) A reassessment of podzol formation processes. *Journal of Soil Science*, **33**, 125–136.

Anderson S.P., Drever J.I. & Humphrey N.F. (1997) Chemical weathering in glaciated environments. *Geology*, **25**, 399–402.

Bain D.C., Mellor A., Wilson M.J. & Duthie D.M.L. (1994) Chemical and mineralogical weathering rates and processes in an upland granitic till catchment in Scotland. *Water, Air, and Soil Pollution*, **73**, 11–27.

Barnhisel R.I. & Bertsch P.M. (1989) Chlorites and hydroxy-interlayered vermiculite and smectite. Pp. 729–788 in: *Minerals in Soil Environments* (J.B. Dixon & S.B. Weed, editors). Soil Science Society of America, SSSA Book Series, no. 1., 2nd Edition, Madison, Wisconsin, USA.

Baroni C. & Carton A. (1990) Variazioni oloceniche della Vedretta della Lobbia (gruppo dell'Adamello, Alpi Centrali). *Geografia Fisica Dinamica Quaternaria*, **13**, 105–119.

Bäumler R. & Zech W. (1994) Soils of the high mountain region of Eastern Nepal: classification, distribution and soil forming processes. *Catena*, **22**, 85–103.

Bishop J., Madejová J., Komadel P. & Fröschl H. (2002) The influence of structural Fe, Al and Mg on the infrared OH bands in spectra of dioctahedral smectites. *Clay Minerals*, **37**, 607–616.

Bockheim J.G., Munroe J.S., Douglass D. & Koerner D. (2000) Soil development along an elevational gradient in the southeastern Uinta Mountains, Utah, USA. *Catena*, **39**, 169–185.

Bosselini A., Castellarin A., Dal Piaz, G.V. & Nardin, E. (2002) *Carta geologica e dei lineamenti strutturali del Trentino*. Servizio Geologico, Provincia Autonoma di Trento.

Carnicelli S., Mirabella A., Cecchini G. & Sanesi G. (1997) Weathering of chlorite to a low-charge expandable mineral in a Spodosol on the Apennine mountains, Italy. *Clays and Clay Minerals*, **45**, 28–41.

Cooper A.W. (1960) An example of the role of microclimate in soil genesis. *Soil Science*, **90**, 109–120.

Dahlgren R.A. & Ugolini F.C. (1991) Distribution and characterisation of short-range-order minerals in Spodosols from the Washington Cascades. *Geoderma*, **48**, 391–413.

Dahlgren R.A., Boettinger J.L., Huntington G.L. & Amundson R.G. (1997) Soil development along an elevational transect in the western Sierra Nevada, California. *Geoderma*, **78**, 207–236.

Dambrine E. (1986) Répartition, morphologie et fonctionnnement des Podzols de haute montagne cristalline sous climat tempéré. Pp. 69–83 in: *Podzols et Podzolisation* (D. Righi & A. Chauvel, editors). Institut National de la Recherche Agronomique, (INRA) et AFES, Paris.

De Coninck F. (1980) Major mechanisms in formation of spodic horizons. *Geoderma*, **24**, 101–128.

Egli M., Mirabella A. & Fitze P. (2001a) Clay mineral formation in soils of two different chronosequences in the Swiss Alps. *Geoderma*, **104**, 145–175.

Egli M., Fitze P. & Mirabella A. (2001b) Weathering and evolution of soils formed on granitic, glacial deposits: results from chronosequences of Swiss Alpine environments. *Catena*, **45**, 19–47.

Egli M., Mirabella A. & Fitze P. (2003a) Formation rates of smectites derived from two Holocene chronosequences in the Swiss Alps. *Geoderma*, **117**, 81–98.

Egli M., Mirabella A., Sartori G. & Fitze P. (2003b) Weathering rates as a function of climate: results from a climosequence of the Val Genova (Trentino, Italian Alps). *Geoderma*, **111**, 99–121.

Egli M., Mirabella A. & Sartori G. (2004) Weathering of soils in Alpine areas as influenced by climate and parent material. *Clays and Clay Minerals*, **52**, 287–303.

FAO (1998) *World Reference Base for Soil Resources.* World Soil Resources Reports 84, FAO, Rome.

Farmer V.C. (1974) Layer silicates. Pp. 331–363 in: *Infrared Spectra of Minerals* (V.C. Farmer, editor). Monograph **4**, Mineralogical Society, London.

Farmer V.C. (1982) Significance of the presence of allophane and imogolite in podzols Bs horizons for podzolization mechanisms: a review. *Soil Science and Plant Nutrition*, **28**, 571–578.

Gjems O. (1967) Studies on clay minerals and clay mineral formation in soil profiles in Scandinavia. *Meddelelser fra det Norske Skogforsöksvesen*, **21**, 303–415.

Gjems O. (1970) Mineralogical composition and pedogenic weathering of the clay fraction in Podzol soil profiles in Zalesine, Yugoslavia. *Soil Science*, **110**, 237–243.

Goodman B.A., Russell J.D., Fraser A.R. & Woodhams F.W.D. (1976) A Mössbauer and IR spectroscopic study of the structure of nontronite. *Clays and Clay Minerals*, **24**, 53–59.

Gustafsson J.P., Bhattacharya P., Bain D.C., Fraser A.R. & McHardy W.J. (1995) Podzolisation mechanisms and the synthesis of imogolite in Northern Scandinavia. *Geoderma*, **66**, 167–184.

Hall K., Thorn C.E., Matsuoka N. & Prick A. (2002) Weathering in cold regions: some thoughts and perspectives. *Progress in Physical Geography*, **26**, 557–603.

Hunckler R.V. & Schaetzl R.J. (1997) Spodosol development as affected by geomorphic aspect, Baraga County, Michigan. *Soil Science Society of America Journal*, **61**, 1105–1115.

Jenny H. (1980) *The Soil Resource*. Springer, New York.

Karathanasis A.D. (1988) Compositional and solubility relationships between aluminum-hydroxy interlayered soil-smectites and vermiculites. *Soil Science Society of America Journal*, **52**, 1500–1508.

Karathanasis A.D. & Harris W.G. (1994) Quantitative thermal analysis of soil materials. Pp. 360–411 in: *Quantitative Methods in Soil Mineralogy*. (J.E. Amonette & L.W. Zelazny, editors). Soil Science Society of America, SSSA Miscellaneous Publication, Madison, Wisconsin, USA.

Klemmedson J.O. (1964) Topofunction of soils and vegetation in a landscape. *American Society of Agronomy*, **5**, 176–189, special publication.

Laffan M.D., Daly J.S. & Whitton T. (1989) Soil patterns in weathering, clay translocation and podzolisation on hilly and steep land at Port Underwood, Marlborough Sounds, New Zealand: classification and relation to landform and altitude. *Catena*, **16**, 251–268.

Lanson B. (1997) Decomposition of experimental X-ray diffraction patterns (profile fitting): a convenient way to study clay minerals. *Clays and Clay Minerals*, **45**, 132–146.

Lundström U.S., van Breemen N., Bain D., van Hees P.A.W., Giesler R., Gustafsson J.P., Ilvesniemi H., Karltun E., Melkerud P.-A., Olsson M., Riise G., Wahlberg O., Bergelin A., Bishop K., Finlay R., Jongmans A.G., Magnusson T., Mannerkosky H.,

Nordgren A., Nyberg L., Starr M. & Tau Strand L. (2000) Advances in understanding the podzolization process resulting from a multidisciplinary study of three coniferous forest soils in the Nordic Countries. *Geoderma*, **94**, 335–353.

Macyk T.M., Pawluk S. & Lindsay D. (1978) Relief and microclimate as related to soil properties. *Canadian Journal of Soil Science*, **58**, 421–438.

Mahaney W.C. (1978) Late-Quaternary stratigraphy and soils in the Wind River Mountains, western Wyoming. Pp. 223–264 in: *Quaternary Soils* (W.C. Mahaney, editor). Geo-Abstracts, Norwich, UK.

Malcolm R.L., Nettleton W.D. & McCracken R.J. (1969) Pedogenic formation of montmorillonite from a 2:1-2:2 intergrade clay mineral. *Clays and Clay Minerals*, **16**, 405–414.

McKeague J.A., Brydon J.E. & Miles N.M. (1971) Differentiation of forms of extractable iron and aluminium in soils. *Soil Science Society of America Proceedings*, **35**, 33–38.

Mirabella A. & Egli M. (2003) Structural transformations of clay minerals in soils of a climosequence in an Italian Alpine environment. *Clays and Clay Minerals*, **51**, 264–278.

Mirabella A. & Sartori G. (1998) The effect of climate on the mineralogical properties of soils from the Val Genova Valley (Trentino, Italy). *Fresenius Environmental Bulletin*, **7**, 478–483.

Mirabella A., Egli M., Carnicelli S. & Sartori G. (2002) Influence of parent material on clay minerals formation in podzols of Trentino – Italy. *Clay Minerals*, **37**, 699–707.

Moore D.M. & Reynolds Jr. R.C. (1997) *X-ray Diffraction and the Identification and Analysis of Clay Minerals*. 2nd edition, Oxford University Press, New York.

Muhs D.R., Bettis E.A., Been J. & McGeehin J.P. (2001) Impact of climate and parent material on chemical weathering in loess-derived soils of the Mississippi river valley. *Soil Science Society of America Journal*, **65**, 1761–1777.

Olis A.C., Malla P.B. & Douglas L.A. (1990) The rapid estimation of the layer charges of 2:1 expanding clays from a single alkylammonium ion expansion. *Clay Minerals*, **25**, 39–50.

Parfitt R.L. & Henmi T. (1982) Comparison of an oxalate-extraction method and an infrared spectroscopic method for determining allophane in soil clays. *Soil Science and Plant Nutrition*, **28**, 183–190.

Pedrotti F., Orsomando E., Francalancia C. & Cortini Pedrotti C. (1974) *Carta della vegetazione del Parco Nazionale dello Stelvio, scala 1:50000*. Dipartimento di Botanica, Università di Camerino.

Rech J.A., Reeves R.W. & Hendricks D. (2001) The influence of slope aspect on soil weathering processes in the Springerville volcanic field, Arizona. *Catena*, **43**, 49–62.

Reynolds R.C. (1971) Clay mineral formation in an alpine environment. *Clays and Clay Minerals*, **19**, 361–374.

Righi D., Huber K. & Keller C. (1999) Clay formation and podzol development from postglacial moraines in Switzerland. *Clay Minerals*, **34**, 319–332.

Sartori G., Mancabelli A., Corradini F. & Wolf U. (2005) *Atlante dei suoli del Parco Adamello-Brenta*. Suoli e paesaggi. Monografie del Museo Tridentino di Scienze Naturali, II, 239 pp.

Sboarina C. & Cescatti A. (2004) *Il clima del Trentino – Distribuzione spaziale delle principali variabili climatiche.* Centro di Ecologia Alpina, Trento.

Schaetzl R.J. & Isard S.A. (1996) Regional-scale relationships between climate and strength of podzolization in the Great Lakes Region, North America. *Catena*, **28**, 47–69.

Schwertmann U. (1964) Differenzierung der Eisenoxide des Bodens durch Extraktion mit Ammoniumoxalat Lösung. *Zeitschrift für Pflanzenernährung, Düngung und Bodenkunde*, **105**, 195–202.

Senkayi A.L., Dixon J.B. & Hossner L.R. (1981) Transformation of chlorite to smectite through regularly interstratified intermediates. *Soil Science Society of America Journal*, **45**, 650–656.

Servizio Idrografico (1959) *Precipitazione medie mensili ed annue per il Trentino 1921-1950.* Istituto Poligrafico dello Stato, Roma.

Tamura, T. (1958) Identification of clay minerals from acid soils. *Journal of Soil Science*, **9**, 141–147.

van Hees P.A.W., Lundström U.S. & Giesler R. (2000) Low molecular weight organic acids and their Al-complexes in soil solution – composition, distribution and seasonal variation in three podzolized soils. *Geoderma*, **94**, 173–200.

Van Ranst E., Stoops G., Gallez A. & Vandenberghe R.E. (1997) Properties, some criteria of classification and genesis of upland forest podzols in Rwanda. *Geoderma*, **76**, 263–283.

Vantelon D., Pelletier M., Michot L.J., Barres O. & Thomas F. (2001) Fe, Mg and Al distribution in the octahedral sheet of montmorillonites. An infrared study in the OH-bending region. *Clay Minerals*, **36**, 369–379.

Whittaker R.H., Buol S.W., Niering W.A. & Havens Y.H. (1968) A soil and vegetation pattern in the Santa Catalina Mountains, Arizona. *Soil Science*, **105**, 440–450.